

DEVELOPMENT OF DE-ICING AND ANTI-ICING SOLUTIONS FOR AIRCRAFT ON
GROUND AND ANALYSIS OF THEIR FLOW INSTABILITY CHARACTERISTICS

A THESIS SUBMITTED TO
THE GRADUATE SCHOOL OF NATURAL AND APPLIED SCIENCES
OF
MIDDLE EAST TECHNICAL UNIVERSITY

BY

DURMUŞ SİNAN KÖRPE

IN PARTIAL FULFILLMENT OF THE REQUIREMENTS
FOR
THE DEGREE OF MASTER OF SCIENCE
IN
AEROSPACE ENGINEERING

SEPTEMBER 2008

Approval of the thesis:

**DEVELOPMENT OF DE-ICING AND ANTI-ICING SOLUTIONS FOR AIRCRAFT ON
GROUND AND ANALYSIS OF THEIR FLOW INSTABILITY CHARACTERISTICS**

Submitted by **DURMUŞ SİNAN KÖRPE** in partial fulfillment of the requirements for
the degree of **Master of Science in Aerospace Engineering Department, Middle East
Technical University** by,

Prof. Dr. Canan Özgen
Dean, Graduate School of **Natural and Applied Sciences**

Prof. Dr. İsmail Hakkı Tuncer
Head of Department, **Aerospace Engineering**

Assoc. Prof. Dr. Serkan Özgen
Supervisor, **Aerospace Engineering Dept., METU**

Assoc. Prof. Dr. Yusuf Uludağ
Co- Supervisor, **Chemical Engineering Dept., METU**

Examining Committee Members:

Prof. Dr. İsmail Hakkı Tuncer
Aerospace Engineering Dept., METU

Assoc. Prof. Dr. Serkan Özgen
Aerospace Engineering Dept., METU

Assoc. Prof. Dr. Yusuf Uludağ
Chemical Engineering Dept., METU

Assoc. Prof. Dr. Göknur Bayram
Chemical Engineering Dept., METU

Asst. Prof. Dr. Oğuz Uzol
Aerospace Engineering Dept., METU

Date:

04.09.2008

I hereby declare that all information in this document has been obtained and presented in accordance with academic rules and ethical conduct. I also declare that, as required by these rules and conduct, I have fully cited and referenced all material and results that are not original to this work.

Name, Last Name : Durmuş Sinan Körpe

Signature :

ABSTRACT

DEVELOPMENT OF DE-ICING AND ANTI-ICING SOLUTIONS FOR AIRCRAFT ON GROUND AND ANALYSIS OF THEIR FLOW INSTABILITY CHARACTERISTICS

Körpe, Durmuş Sinan

M.S., Department of Aerospace Engineering

Supervisor : Assoc. Prof. Dr. Serkan Özgen

Co-Supervisor: Assoc. Prof. Dr. Yusuf Uludağ

September 2008, 79 Pages

In this thesis, development process of de-icing and anti-icing solutions and their flow instability characteristics are presented.

In the beginning, the chemical additives in the solutions and their effects on the most critical physical properties of the solutions were investigated. Firstly, chemical additives were added to glycol and water mixtures at different weight ratios one by one in order to see their individual effects. Then, the changes in physical properties were observed when the chemicals were added to water-glycol mixture together. After that, study was focused on effect of polymer which makes the solution pseudoplastic. Further investigations on viscosity behavior of the solution at different pH values, glycol and water mixtures and surfactant weight ratios, which is used for surface tension reduction, were performed.

For the investigation of flow instability characteristics of the solutions' flows, linear stability analysis for two-layer flows is a basic tool. Firstly, the effects of main parameters on the stability of two-layer flows were observed with a parametric study. Then, the commercially available and developed de-icing and anti-icing solutions were compared according to the characteristics of unstable waves. According to the results, unstable waves on developed de-icing fluids are observed at a lower critical wind speed compared to the commercially available de-icing solution. Moreover, it flows off the wing faster due to a higher value of critical wave speed. Developed anti-icing solution has similar wave characteristics compared to commercially available anti-icing solution, except critical wave speed, which is significantly lower. However, this problem can be overcome by decreasing the viscosity of developed anti-icing solution at very low shear rates.

Keywords: De-Icing Solutions, Anti-Icing Solutions, Two-Layer Flows, Linear Stability Theory, Rheology.

ÖZ

YERDEKİ UÇAKLAR İÇİN BUZLANMAYI GİDEREN VE BUZLANMAYI ÖNLEYEN SIVILARIN GELİŞTİRİLMESİ VE AKIŞ KARARSIZLIK ÖZELLİKLERİNİN İNCELENMESİ

Körpe, Durmuş Sinan

Yüksek Lisans, Havacılık ve Uzay Mühendisliği Bölümü

Tez yöneticisi : Yrd. Doc. Dr. Serkan Özgen

Yardımcı tez yöneticisi : Yrd. Doc. Dr. Yusuf Uludağ

Eylül 2008, 79 sayfa

Bu tezde, buzlanma giderici ve önleyici çözeltilerin geliştirilmesi süreci ve akışlarının kararsızlık özellikleri sunulmaktadır.

Başlangıçta, çözeltiler içindeki kimyasal katkıların ve bunların çözeltilerin en önemli fiziksel özelliklerine olan etkileri incelenmiştir. İlk olarak kimyasal katkıları, farklı ağırlık oranlarında glikol ve su karışımlarına eklenmiş birer birer eklenmiş ve başlı başına etkileri incelenmiştir. Daha sonra, fiziksel özelliklerdeki değişimler kimyasallar çözeltiliye hep birlikte eklendiğinde incelenmiştir. Bundan sonra, çalışma sıvısının psedoplastik olmasını sağlayan polimer üzerine yoğunlaşmıştır. Farklı pH değerlerinde, glikol ve su karışımlarında ve yüzey aktif madde ağırlık oranlarında çözeltilerin viskozitelerinin davranışları incelenmiştir.

İki katmanlı akışlar için doğrusal kararlılık teorisi, çözeltilerin akışının kararsızlık özellikleri incelemek için temel bir araçtır. İlk olarak iki katmanlı akışlar içindeki temel parametrelerin iki katmanlı akışların kararlılığına etkisi parametrik bir çalışmayla incelenmiştir. Daha sonra, ticari olarak temin edilebilen ve geliştirilmiş buzlama giderici ve önleyici sıvıların, kararsız dalga özellikleri karşılaştırılmıştır. Elde edilen sonuçlara göre, geliştirilmiş olan buzlanma giderici sıvıdaki dalga oluşumu temin edilebilir sıvıya göre daha düşük hızlarda görülmektedir. Üstelik, kritik dalga hızının daha yüksek olması nedeniyle, kanat yüzeyinden daha hızlı ayrılır. Geliştirilmiş buzlanma önleyici sıvı ise temin edilebilir buzlanma önleyici sıvıyla, dikkat çeker bir seviyede daha az olan kritik dalga hızı hariç, benzer dalga özellikleri göstermektedir. Ancak, geliştirilmiş sıvının düşük kayma hızlarında oluşan viskozitesini azaltarak, bu sorunun üstesinden gelinilebilir.

Anahtar Kelimeler: Buzlanma Giderici Sıvılar, Buzlanma Önleyici Sıvılar, İki Katmanlı Akışlar, Lineer Kararlılık Teorisi, Reoloji.

ACKNOWLEDGEMENTS

I would like to express my gratitude to my supervisor Assoc. Prof. Dr. Serkan Özgen, for his support and guidance throughout the study.

I also would like to thank Assoc. Prof. Dr. Yusuf Uludağ and Assoc. Prof. Dr. Göknur Bayram for their support, encouragement, criticism and comments.

Thanks to Prof. Dr. Niyazi Bıçak for his support to the project and teaching us how a scientist and inventor should be.

Thanks to Barış Erdoğan for help that I need during two years of study. It would never be possible without his support.

Thanks to my fiancée, Didem, for his endless love and support. She is an angel living on the earth.

Thanks to my nephew, Ali Rıza, for his delphic but enjoyable speeches on the phone.

Thanks to Bıçak Laboratory students; Bünyas, Burcu and Deniz. Despite I broke lots of beakers and asked many ridiculous questions, they were always helpful and polite to me.

Thanks to my family and my “new” family, for their support and patience.

Thanks to my friends, Adem, Umut and Utku, just for being my friends.

Thanks to the assistants and technicians of Chemistry and Chemical Engineering Department of METU and Chemistry Department of İTÜ for their support to this project.

This study was supported by a grant by TÜBİTAK with a project number 106M219.

TABLE OF CONTENTS

ABSTRACT.....	iv
ÖZ.....	vi
ACKNOWLEDGEMENTS.....	viii
TABLE OF CONTENTS.....	ix
LIST OF TABLES.....	xii
LIST OF FIGURES.....	xiii
LIST OF SYMBOLS.....	xvi
CHAPTER	
1. INTRODUCTION.....	1
1.1 Motivation.....	1
1.2 Background of the study.....	2
1.3 Road map.....	8
2. DEVELOPMENT OF DE-ICING AND ANTI-ICING FLUIDS.....	10
2.1 Literature research.....	10
2.2 Development of de-icing solutions.....	12
2.3 Development of anti-icing solutions.....	16

2.3.1 Polymer concentration effect	17
2.3.2 pH effect.....	18
2.3.3 Glycol-water concentration effect	19
2.3.4 Surfactant effect.....	20
3. MATHEMATICAL MODEL AND SOLUTION METHOD FOR THE LINEAR STABILITY ANALYSIS OF TWO-LAYER FLOWS	23
3.1 Objective	23
3.2 Introduction.....	23
3.3 Derivations of the Orr-Sommerfeld equations.....	27
3.3.1 Method of small disturbances	28
3.3.2 Method of normal modes	31
3.4 Two-layer flow.....	33
3.4.1 Laminar and turbulent boundary layer	35
3.5 Solution method.....	36
4. RESULTS AND DISCUSSION	40
4.1 Objective	40
4.2 Results obtained by using laminar boundary layer	40
4.2.1 Validation of the method.....	40
4.2.2 Parametric study	42
4.3 Results obtained by using turbulent boundary layer.....	50

4.3.1. Validation of the method.....	50
4.3.2 Wave characteristics of de-icing and anti-icing solutions.....	52
5. CONCLUSIONS AND RECOMMENDATIONS.....	58
5.1 General conclusions.....	58
5.2 Recommendations for better solutions	60
5.3 Recommendations for future work.....	61
REFERENCES.....	62
APPENDICES	
A. DERIVATION OF INTERFACE CONDITIONS FOR TWO-LAYER FLOW	66
B. DENSITY AND SURFACE TENSION MEASUREMENTS.....	70
C. NEUTRAL STABILITY CURVES FOR SAMPLE FLUIDS AT DIFFERENT THICKNESSES AND TEMPERATURES.....	75

LIST OF TABLES

Table 2.1 Viscosity, surface tension and freezing point values of glycol and water mixture	13
Table 2.2 Names and concentration ranges of chemical additive groups.....	14
Table 2.3 Effects of functional chemicals on physical properties of Type-1 solutions.....	14
Table 2.4 Effects of chemical additives on physical properties of Type-1 solutions when they are used together	15
Table 2.5 The final composition of de-icing fluid by weight and its physical properties	16
Table 4.1 Physical properties of the de-icing solutions that are used in the analysis at different temperatures.	53
Table 4.2 Physical properties of the anti-icing solutions that are used in analysis at different temperatures.	53
Table 4.3 Physical properties of air at different temperatures.	54
Table 4.4 Wave characteristics of T1 solution.	55
Table 4.5 Wave characteristics of G1 solution.	55
Table 4.6 Wave characteristics of T2 solution.	56
Table 4.7 Wave characteristics of G1 solution.	56

LIST OF FIGURES

Figure 1.1 Approximate effect of wing upper surface ice contamination on the stall speed of a typical small turbojet transport	3
Figure 1.2 The simulation of FPET [7].....	5
Figure 1.3 Determination of acceptance criteria [7].....	6
Figure 2.1 Rheological behavior of 1% of HMPA solutions by weight.....	17
Figure 2.2 Rheological behavior of 2% of HMPA solutions by weight.....	18
Figure 2.2 Rheological behavior of 4% of HMPA solutions by weight.....	18
Figure 2.3 Rheological behavior of 4% of HMPA solutions by weight.....	18
Figure 2.4 The change of zero shear viscosity of the 0.075 wt % HMPA solutions composed of 50 % water and 50 % glycol with pH.....	19
Figure 2.5 The rheological behavior of HMPA solutions at 0.064 wt % concentration with different glycol-water content.	20
Figure 2.6 The surface tension change of HMPA solution (0.067 wt %) with addition of AOT.....	21
Figure 2.7 The viscosity change of HMPA solution (0.067 wt %) with addition of AOT.....	22
Figure 3.1 Sketch of laminar-turbulent transition [24].....	24

Figure 3.2 Flow system geometry.....	33
Figure 4.1 Amplification rate for Yih's case for TS mode ($m = 598802, r = 972,$ $l = 3.5668, S = 0.1027, F = 496, R = 678$).....	41
Figure 4.2 Neutral stability curves for the two instability modes ($m = 5, l = 0.5,$ $r = 1, S = 0, F = 0$).....	42
Figure 4.3 α_{cr} and Re_{cr} on TS neutral stability curve ($m = 10, l = 1, r = 1, S = 0,$ $F = 0$).....	43
Figure 4.4 Effect of viscosity ratio m ($l = 1, r = 1, S = 0, F = 0$).	44
Figure 4.5 Effect of thickness ratio l ($m = 5, r = 1, S = 0, F = 0$).....	45
Figure 4.6 Effect of density ratio r ($m = 5, l = 0.5, S = 0, F = 0$).	46
Figure 4.7 Effect of density ratio r on TS mode ($m = 5, l = 0.5, S = 0, F = 0$).	47
Figure 4.8 Effect of surface tension parameter S ($m = 5, l = 0.5, r = 1, F = 0$).....	48
Figure 4.9 Effect of Froude number F ($m = 5, l = 0.5, S = 0, r = 1$).	49
Figure 4.10 Effect of n ($m = 5, l = 0.5, S = 0, F = 0, r = 1$).....	50
Figure 4.11 Amplification rate for Miesen and Boeresma's case for TS mode ($m = 56.4, r = 824, T^* = 0.074 \text{ mN/m}, F = 1061$).....	51
Figure 4.12 Result of Miesen and Boeresma's work for TS mode ($m = 56.4, r = 824,$ $T^* = 0.074 \text{ mN/m}, F = 1061$) [33].	52
Figure B.1 Variation of density with temperature for T1 fluid.....	71
Figure B.2 Variation of density with temperature for T2 and G2 fluids.....	71
Figure B.3 Variation of density with temperature for G1 fluid.....	72
Figure B.4 Variation of surface tension with temperature for T1 fluid.....	72

Figure B.5 Variation of surface tension with temperature for T2 fluid.....	73
Figure B.6 Variation of surface tension with temperature for G1 fluid.....	73
Figure B.7 Variation of surface tension with temperature for G2 fluid.....	74
Figure C.1 Neutral stability curves for $d_2^* = 2.4$ mm. at 20 °C for sample fluids. ...	75
Figure C.2 Neutral stability curves for $d_2^* = 1.8$ mm. at 20 °C for sample fluids. ...	76
Figure C.3 Neutral stability curves for $d_2^* = 1.2$ mm. at 20 °C for sample fluids. ...	76
Figure C.4 Neutral stability curves for $d_2^* = 2.4$ mm. at 0 °C for sample fluids.....	77
Figure C.5 Neutral stability curves for $d_2^* = 1.8$ mm. at 0 °C for sample fluids.....	77
Figure C.6 Neutral stability curves for $d_2^* = 1.2$ mm. at 0 °C for sample fluids.....	78
Figure C.7 Neutral stability curves for $d_2^* = 2.4$ mm. at -20 °C for sample fluids.	78
Figure C.8 Neutral stability curves for $d_2^* = 1.8$ mm. at -20 °C for sample fluids.	79
Figure C.9 Neutral stability curves for $d_2^* = 1.2$ mm. at -20 °C for sample fluids.	79

LIST OF SYMBOLS

Superscripts

- ' Derivation with respect to dimensionless normal distances y
- * Dimensional quantities
- ^ Disturbance components

Subscripts

- 1 The quantities for upper layer
- 2 The quantities for lower layer
- 0 The quantities for interface
- e The quantities at the interface
- i Imaginary part of a complex quantity
- r Real part of a complex quantity
- cr Quantities at critical conditions

Greek Symbols

- α Wave number
- α_i Imaginary part of a complex wave number
- α_r Real part of a complex wave number–spatial growth rate
- β Defined as $\beta^2 = \alpha^2 + i\alpha R(1 - c)$
- λ Wavelength
- μ^* Dynamic viscosity
- ν^* Kinematic viscosity
- φ Disturbance velocity amplitude function for upper fluid
- χ Disturbance velocity amplitude function for lower fluid
- λ Disturbance hydrostatic pressure amplitude function
- ρ^* Density
- σ^* Normal stress component
- σ Temporal growth rate
- τ^* Shear stress component
- ξ^* Shear stress component

Alphanumeric Symbols

C_f	Skin friction coefficient
F	Froude number
P	Mean hydrostatic pressure
R	Reynolds number
S	Surface tension parameter
T	Surface tension coefficient
U	Mean streamwise Cartesian velocity component
V	Mean normal Cartesian velocity component
c	Complex wave velocity
c_i	Imaginary part of a complex wave velocity-temporal growth rate
c_r	Real part of a complex wave velocity-phase speed
d	Reference length
f	Dimensionless stream function in Falkner-Skan equation
g	Gravitational acceleration
k	Consistency factor for power-law fluids
l	Depth ratio of fluids
m	Viscosity ratio
n	Power-law index
p	Total hydrostatic pressure
\hat{p}	Disturbance hydrostatic pressure
r	Density ratio
t	Time
u	Total streamwise Cartesian velocity component
\hat{u}	Streamwise disturbance velocity component
v	Total normal Cartesian velocity component
\hat{v}	Normal disturbance velocity component
x	Streamwise Cartesian coordinate
y	Normal Cartesian coordinate

Abbreviations

FPET Flat plate elimination test

BLDT Boundary layer displacement thickness

LOUT Lowest operational use temperature

HMPA hydrophobically modified polyacrylic acids

TS Tollmien-Schlichting

CHAPTER 1

INTRODUCTION

1.1 Motivation

The history of winter operations shows that de-icing and anti-icing operations play a vital role in flight safety. Since de-icing and anti-icing operations are worldwide issues, many organizations and companies contributed with valuable research to icing related problems.

Development and production of de-icing and anti-icing solutions are very sophisticated issues, since standards have been prepared for extreme conditions. The standards focus on three main categories:

- 1) Performance of de-icing and anti-icing solutions on aircraft surface,
- 2) Effect of the solutions on aircraft performance,
- 3) Compatibility of the solutions with materials that aircraft is made of and environment.

Moreover, these standards and regulations are rearranged regularly in order to make the companies produce new technologies for the solutions.

Development of de-icing and anti-icing solutions requires deep knowledge in Chemistry. To find the most effective chemicals and chemical ratios in the solutions necessitates preparing a great number of sample solutions and measuring their physical properties, such as viscosity, surface tension and freezing point. In addition to this, the chemical that is used for changing a physical property may affect other physical properties. This makes the development process more complicated.

Since de-icing and anti-icing solutions have a wavy surface during takeoff, air flow over surface of aircraft is disturbed. Therefore, the disturbance mechanism should be carefully understood. Since experimental investigation is very expensive, flow system should be sim-

ulated by using mathematical modeling.

The benefit of this study can be seen in three different aspects. In Chemical Engineering aspect, the main objective of this study is to find chemical additives and composition ratios to get the desired physical properties, especially viscosity, surface tension and freezing point that are very important for the design of de-icing and anti-icing solutions.

In Aerospace Engineering aspect, the main aim is to find the wave characteristics of the developed de-icing and anti-icing solutions and compare the result with the results of commercially available solutions.

Finally, in economical aspect, the developed solutions will be produced locally. In addition to this, a strong background will be constructed for icing problem that is observed on railways and highways.

1.2 Background of the study

De-icing and anti-icing solutions still have important roles in aircraft ground operations in order to satisfy the FAR 91.209 and FAR 121.629 requirements, which have been announced by the Airworthiness Authorities strongly stating that an aircraft's surface must be cleaned from ice, frost and snow contamination before takeoff [1]. The mentioned rules are very crucial to obey in order to prevent adverse effects of ice, frost and snow contamination. These effects can be seen in four forces that an aircraft is subject to, namely Lift, Drag, Thrust and Weight. Due to frost, snow, slush or ice accretion, lift decreases, drag increases, available excess thrust decreases and weight increases. The wing, vertical and horizontal stabilizers are designed to direct the airflow in a particular way and any contamination will disturb this flow. As a result, there will be an early flow separation that will cause an unpredicted lift loss. Surely, the contamination also increases the drag. Moreover, the location of the contamination does not necessary have to be on the wing. The contamination on the fuselage also causes increase in drag. During take-off, when a thin layer of contamination is on the wing, maximum angle of attack is decreased and this causes an unexpected and early stall. In order to prevent this, the velocity of aircraft is increased. Thrust must always be added (if excess thrust is available) to compensate for the reduced performance [2]. Figure 1.1 shows the estimation for the stall speed increase

due to contamination that would occur on small turbojet transports like the B737, and DC-9.

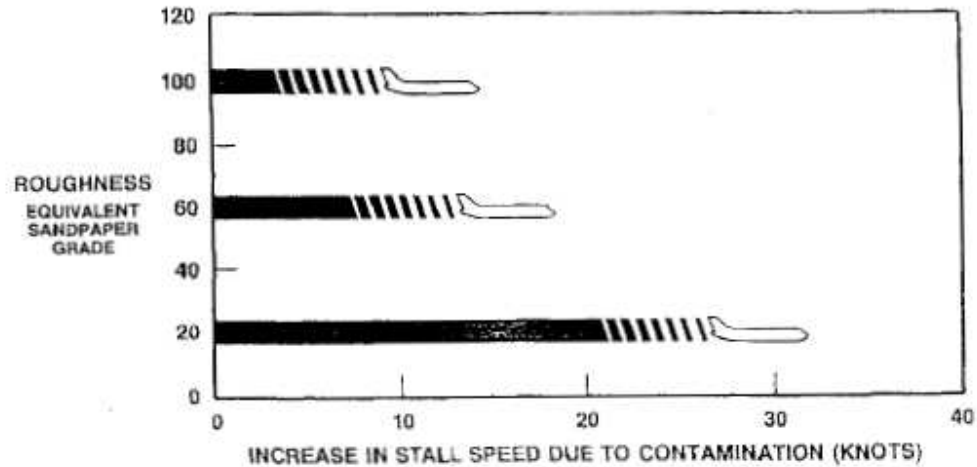


Figure 1.1 Approximate effect of wing upper surface ice contamination on the stall speed of a typical small turbojet transport.

In Figure 1.1, equivalent sandpaper grade describes the grade of Coated Abrasives Manufacturer's Institute (CAMI). The smaller sandpaper grade has the bigger average particle size in microns. Therefore, it creates rougher surface when it is adhered to the wing.

Preventing the adverse effects of ice, frost and snow contamination that are mentioned above become a major airline operation problem due to negative economical effects of interruptions of flight schedules due to bad weather conditions [3].

In order to prevent this, glycol-based de-icing and anti-icing solutions have been used especially in North America and Northern Europe since the 1930s. The main reason for the utilization of glycols is the fact that they are freezing-point depressants [4].

The main surfaces that the de-/anti-icing solutions are applied are:

- a) Wing upper surfaces and leading edges,

- b) Horizontal stabilizer upper surfaces including leading edges and elevator upper surfaces,
- c) Vertical stabilizer and rudder,
- d) Fuselage upper surfaces [2].

There are four types of de/anti-icing solutions. Type-I fluids are around 80% glycol based fluids that are used in order to remove ice contamination from the airplane surface. In other words they are de-icing fluids. They are Newtonian fluids and their holdover time, which is defined as the period of time a fluid will protect a treated surface against freezing in defined winter weather conditions, is low. Moreover, they include some chemicals for surface tension reduction, corrosion prevention and pH independency, etc. Type-II/-III/-IV fluids are pseudoplastic fluids which have viscosities that are dependent on both temperature and shear rate. The main difference between Type-I fluids and pseudoplastic fluids are the polymers that the pseudoplastic fluids contain. Polymers make the solution pseudoplastic and allow the solution to have very high viscosity compared to Type-I fluids especially at low shear rates. With the help of this pseudoplastic behavior, these fluids have higher holdover times.

Although the de-icing and anti-icing solutions are being used for more than half a century, the specifications and standards related to de-icing and anti-icing fluids were started to be outlined only after the accident in 1982 in Washington D.C. [5]. After the disaster, preliminary investigations revealed that ice changed the thrust settings in order to climb, increased drag, decreased maximum lift coefficient and changed the handling characteristics [5]. Moreover, the tests which were performed by Boeing showed that all of the de-icing and anti-icing fluids that were being used around the world at that time were unable to leave the aircraft surface easily during takeoff. As a result, they caused a decrease in aircraft performance, sometimes more than the ice contamination itself.

Nature of lift loss mechanism that was understood in these experiments is defined as follows: the wavy solution layer at bottom causes an increase on the roughness of the wing surface. This situation makes the airflow boundary layer thicker. Moreover there exists an energy transfer from air to the solution which also causes thicker boundary layer. This modifies the shape of the wing by an amount equivalent to the displacement thickness [6].

After the terrifying results of the test, the aviation associations agreed to prepare aerodynamic acceptance standards in order to enforce the de-icing and anti-icing producers develop new technologies. In order to do this, flight tests and 3-D model wind tunnel tests were performed between 1988 and 1990 in Finland and in NASA Ice Research Laboratory in USA, respectively [6].

In wind tunnel tests, the take-off simulations of the flight tests were performed. When the results were compared, it was found out that the lift coefficients matched each other with an error of 1.5 %. Finally, the maximum tolerable lift coefficient loss for a wing on which the de-icing and anti-icing fluids are applied was found as 5.24 % compared to a clean wing. Due to the high cost of 3-D model tests, the correlation between the flight tests and flat plate was declared. This test is defined as flat plate elimination test (FPET). A typical result obtained from such a test is shown in Figure 1.2.

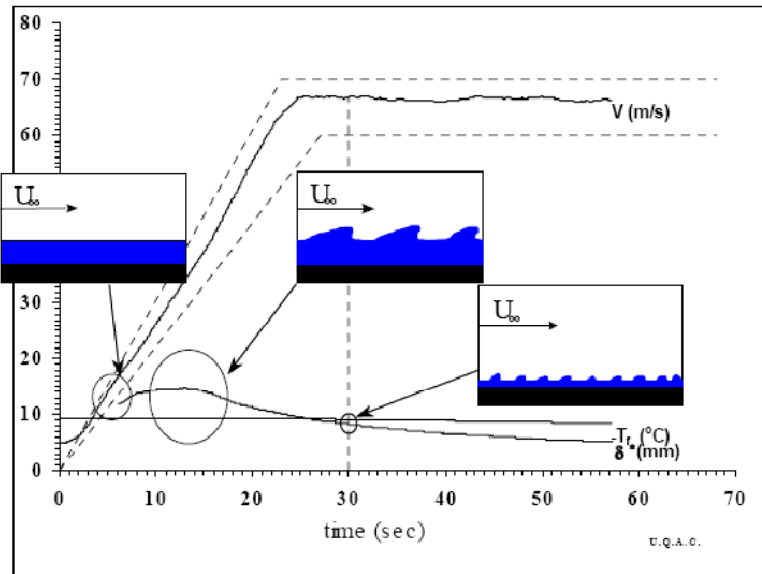


Figure 2.2 The simulation of FPET [7]

In Figure 1.2 variation of boundary layer displacement thickness (BLDT) with speed is depicted. Values in y axis show tunnel speed in m/s and BLDT in mm. As it is seen, at low speeds there is no wave observation on de-icing fluid layer. As speed increases waves are observed that cause thicker BLDT. As speed further increases beyond a threshold value,

BLDT starts decreasing. This situation probably occurs due to decrease in fluid thickness. Moreover test results of other solutions revealed that initial solution thickness, which is one of test parameters, does not influence the final thickness [6]. According to these, the boundary layer displacement thickness on a plate that is covered with de-icing and anti-icing fluids must be less than 10 mm. at -20°C , which was obtained in the tests that were performed with the solution described by Military specification 8243-D, so that the lift loss shall stay within limits. The example of determination of acceptable BLDT is in Figure 1.3.

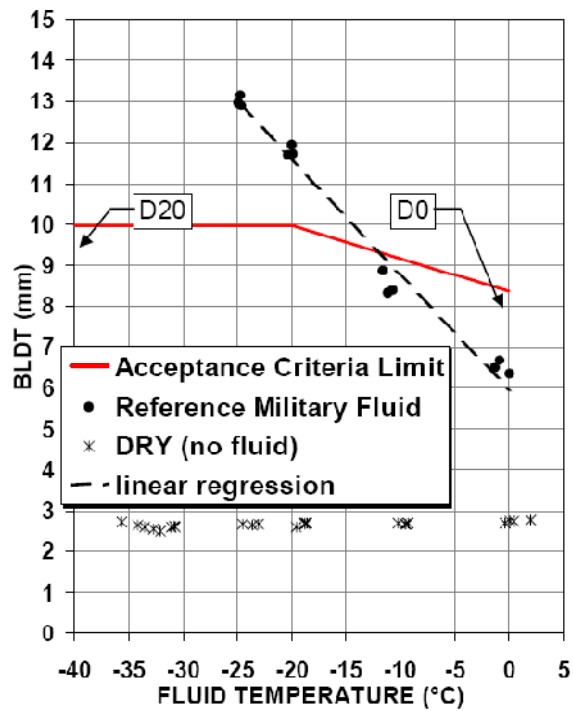


Figure 3.3 Determination of acceptance criteria [7]

As it is seen, BLDT acceptance value remains constant for temperatures less than -20°C . As temperature increases, the value of acceptable BLDT decreases. Moreover, In Figure 1.3, D20 and D0 show the values of BLDT of a sample fluid at -20°C and 0°C , respectively.

In addition to aerodynamic acceptance standards, the new standards are decided for performance of de-icing and anti-icing fluids. These are mainly related to the protection time of de-icing and anti-icing fluids against contamination. For these standards, simulations of weather conditions such as active frost, snow, freezing drizzle, etc. are

performed. Then, the protection time of the developed or available de/anti-icing solutions are found. Since the application of these solutions is a difficult task, the standards related to the application processes of these solutions are decided.

After these standards were outlined, the producers started to develop new de-icing and anti-icing fluids using newer technologies according to the American Society for Testing and Material (ASTM) 1424 and 1428 performance standard needs. The main physical, rheological and performance properties of the solutions are defined in these standards are as follows:

Viscosity:

Viscosity is a measure of the resistance of a fluid when it is being deformed by a stress. De-icing and anti-icing solutions should have the desired viscosities and behaviors in order to meet the protection standards [7]. Due to variation of viscosity according to the stress that is applied, the viscometer model and spindle number should be defined during measurements and comparison.

Surface tension:

De-icing and anti-icing solutions should have a surface tension around 35 mN/m in order to provide rapid and uniform wetting and spreading on the aircraft surface in order to satisfy better application requirements [7].

Freezing Point:

For solutions, there is no significant temperature at which the freezing starts. Therefore, beginning of crystallization can be defined as the freezing point for a solution. The addition of water due to the contamination or precipitation raises the freezing temperature. Therefore, check of the freezing point should be performed at defined periods.

Lowest Operational Use Temperature (LOUT):

It is defined as the higher of:

- 1) The lowest temperature at which the solution meets the aerodynamic acceptance test or,
- 2) The freezing point of the solution plus 7°C.

According to the regulations, the solutions must not be used if the ambient or aircraft surface temperature is below LOUT [8].

pH:

The value of the pH has a crucial importance in case of the changes in physical and rheological values. Therefore, the pH value of the de-icing and anti-icing solutions should be between 8.5 and 9.5 [7, 8].

In addition to performance and acceptance standards, there are requirements related with the compatibility of the solutions with major airframe structures. Since aircraft are produced using complex materials and considering normal flight conditions, all chemical products have to be tested for compatibility when in contact with these materials. These tests include several scenarios related to fluid compatibility such as corrosion, flammability, embrittlement (hardening and weakening of a solid substance due to age or exposure to extreme conditions), stability etc. [2]. In addition to this, the mentioned compatibility tests are performed for the apparatus that are used during application such as, storage tanks, pipes, hoses, etc [9].

Moreover, there are strong requirements related to the adverse effects of the solutions to the environment. It is known that when the glycol is mixed with water it degrades, but it uses oxygen in water with a ratio between 1.5 and 1.8 of its weight. In order to save the aquatic life and plant habitats, biodegradability and toxicity should be within the strictly defined values [8, 10].

1.3 Road map

This thesis aims to present development of de-icing and anti-icing solution process and study the wave characteristics of these solutions by using linear stability theory. Since solutions are sheared by the air flow, two-layer flow approach is quite suitable for the simulation of the flow system.

Chapter 2 describes development of de-icing and anti-icing solutions in detail. Before the development process, the evolution of the solutions is explained with a patent research. Although the exact chemical composition ratios of the solutions are given in patents, some

of the chemicals are used in order to mislead the people who imitate or copy the solutions. Then, development process of de-icing solutions is defined. In this part, the variation of the physical properties of the solutions with addition of chemical additives is discussed. Initially, the variations are observed by adding the chemicals in solutions one by one at different glycol water mixtures. After that, the variations are discussed when additives are dissolved in the solutions together. Eventually, with the help of results and discussions, a sample final composition is decided. Next, the study is focused on anti-icing solutions. Since the only different between de-icing solution composition and anti-icing solution composition is the addition of polymer, the effect of polymer ratio is investigated initially. Since the most important physical property is viscosity, the change of viscosity with pH and different glycol water mixture is investigated. Afterwards, the effect of surfactant on surface tension and viscosity is investigated. Since, a final composition for anti-icing solution is not ready exactly, it is not declared.

Chapter 3 is devoted to mathematical model and solution method of linear stability theory for two-layer flows. After a literature survey on stability analysis and two-layer flows, the methodology of derivation of Orr-Sommerfeld equations is given. After that, laminar and turbulent boundary layers that define the velocity profile of the upper fluid are discussed. Finally, the solution method is explained.

In Chapter 4, the results of the simulations are discussed. Firstly, the results of parametric study that are obtained by using laminar boundary layer for air are given. In this part, an artificial lower fluid is used and results are obtained by changing one physical property of the artificial fluid but keeping the others constant. As a result, the effects of physical properties on the stability are observed for different neutral stability curves. In the second part, the wave characteristics of developed and commercially available solutions are obtained by using turbulent boundary layer air. The measurements of physical properties of the solutions were performed in the project laboratory, except density. Since glycol and water mixture has a composition ratio of 90-95% in the solutions, for density measurements, the solutions were assumed to be made up of only glycol and water.

Chapter 5 is devoted to the general conclusions that are drawn from the study and recommendation for the future work.

CHAPTER 2

DEVELOPMENT OF DE-ICING AND ANTI-ICING FLUIDS

2.1 Literature research

There are a lot of patents in the literature related to de-/anti-icing solutions. The main reason why we concentrate on them is to investigate the effects of chemical additives on the physical properties of the solutions. This analysis is given in chronological order so that evolution of the solutions is observed.

In the patent numbered 4358389, it is stated that optimum rheological behavior is important because it is the precondition for desired holdover time, flow-off properties during takeoff, handling and spraying the solutions without problem. In the patent, there is detailed information about the composition ratios and the experimental results that are obtained with composition rate based samples [12].

In the patent numbered 4744913, there is extended information about the substances that the new agent comprises. These are glycols, thickeners, corrosion inhibitors, surfactants, neutralizing agents. Firstly, a composition according to the U.S Pat. No.4358389 was prepared. The composition displays laminar flow behavior and required holdover time values and it also satisfies the present requirement for viscosity at very low shear rate of 0.08 1/s up to -15 °C. However, its viscosity at the low shear rate is considerably above the values required at temperatures lower than about -15°C. The known agent had a viscosity considerably above 50000 mPas (according to the regulations of the Association of European Airlines this viscosity must not exceed 50000 mPas). This is defined as a bad characteristic for flow-off. Fortunately, it is found that the disadvantage of the fluid can be removed by using additional thickeners and pH agents. After this part, there is detailed information about the weight composition and chemical composition of the substances. During the decision of the substances, some other U.S patents are applied. Then, the

preparation of the agent and order of adding the substitutes, is defined. After this, there are 6 examples of the agent which are obtained by the changing the weight (exact) ratios of the substances. Then, pH value, viscosity and holdover times of them are calculated. It is stated that the new solution has a viscosity lower than 50000 mPa.s at -25 °C and very low shear rate of 0.08 seconds⁻¹ [13].

In the patent numbered 5118435, the main objectives of the inventions are defined as follows: to provide an antifreeze composition that can retain high viscosity as the composition is diluted with water and to provide an antifreeze composition which under low shear conditions having a viscosity that is relatively insensitive to temperature changes over the range of -25°C to 20°C. After that, there are 4 examples of the fluid by changing the weight (exact) ratios of the substances. The tests are related with viscosity both in neat and in diluted form. The most striking result is defined as having a higher viscosity when the solution is diluted with water [14].

In the patent numbered 5389276, the main motivation is defined as adding polymer to a de-icing fluid in order to increase its protection time. It is also said that the new product will be less corrosive. After that there are 11 examples of the fluid by changing the weight (exact) ratios of the substances. The tests are related with holdover time, wetting ability, viscosity and storage. It is seen that some of the examples had stable foam when they are agitated. Moreover, after two-weeks of storage, precipitation is observed on some of the samples [15].

In the patent numbered 5435930, it is stated that the new solution is prepared for environmental concerns. For this, Potassium Acetate is used instead of glycol. In 3 examples of the solution, boundary layer displacement thicknesses were measured [16].

In the patent numbered 7037442, the objective is to have an improved de-icing and anti-icing solution in which the pseudoplastic behavior is obtained by using water soluble sheet silicate. In 7 examples of the invention, the viscosity measurements reveal that if the prior arts' polymers are used with sheet silicate, much better viscosity behavior is obtained compared to the previous solutions. Moreover, the protection of the surface against icing is better than the previous ones. However, there is no information about material compatibility and environmental effects [17].

According to the patents that are investigated, the chemicals which are in de-icing and anti-icing solutions in weight percent are defined as follows:

- I. 45-65 % glycol
- II. 35-65 % water
- III. 1 ppm -2 % surfactant
- IV. 1 ppm-0.5 % pH controller
- V. 1 ppm-4 % corrosion inhibitor
- VI. 1 ppm-0.5 % foam reducing agent
- VII. 10 ppb-1 % dye
- VIII. 0.1-5 % thickening polymer.

In the current study, the characterization tests of the de icing and anti-icing solutions were performed using a rheometer, a surface tensiometer and a refrigerator:

Rheometer

The rheological behaviour of the polymer solutions was tested by using the Brookfield Rheometer Model LVDV-III U with a spindle no: 34 in a small sample adapter and a temperature bath.

Surface Tensiometer

The surface tension of the solutions was tested by using Cole Parmer Surface Tensiomat 21 with a platinum-iridium ring (circumference: 5.965 cm)

Refrigerator

The freezing point of the solutions was tested by using Revco Ult350-5V-32 refrigerator with -40°C minimum temperature range. For lower temperature measurements, the refrigerator at Food Engineering, METU, which has a lowest operation point of -80°C, was used.

2.2 Development of de-icing solutions

As mentioned above, Type I solutions are used in order to remove ice, snow and frost contamination on the surfaces. Most of the composition is water and glycol. During the

experiments, despite its low viscosity, ethylene glycol is used in the solutions due to its high freezing point depression and its fast biodegradability [18]. Therefore, these experiments are started with the variation of viscosity, surface tension and freezing point of water glycol mixture. The results are shown in Table 2.1.

According to the Table 2.1, viscosity of the solution increases as the ethylene glycol/water weight ratio is increased. Moreover, the surface tension decreases for the same condition. The most striking result is related with the freezing point. Although, the pure ethylene glycol has a freezing point of -12 °C, in the mixture with 70 % and 30 % ethylene glycol and pure water by weight, respectively, the crystallization is observed below -51 °C.

Table 2.1 Viscosity, surface tension and freezing point values of glycol and water mixture

Glycol (wt %)	Water (wt %)	Viscosity (cP) (@20 °C)	Surface Tension (mN/m) (@ 25 °C)	Freezing Point (°C)
100	0	16	49	- 12
90	10	13.9	51.6	- 29
80	20	9.4	52.1	- 46
70	30	6.7	55.5	< - 51
0	100	1	72	0

If the effects of the chemical additives in the solution are considered:

- a) Surfactant: To lower to surface tension of the solution so that the solution spreads over the surface rapidly and uniformly (better wetting characteristics),
- b) Corrosion inhibitor: To protect the surface from corrosion,
- c) pH controller: To make the pH of the solution stay in a desired range.

With the help of patent analysis, three chemicals were decided to be used. The group, chemical name and concentration range is tabulated in Table 2.2.

These chemicals were added to the solution in order to see their effects on viscosity, surface tension and freezing point of the solution. Therefore, the exact amount of additives in solution was not a concern. The results are in Table 2.3.

Table 2.2 Names and concentration ranges of chemical additive groups

Group	Chemical name	Concentration range (wt %)
Surfactant (S)	2-Ethoxyphenol	0 – 2
Corrosion Inhibitor (C)	Tributylamine	0 – 4
pH Controller (pH)	Potassium hydrogen phosphate trihydrate	0 – 0.5

Table 2.3 Effects of functional chemicals on physical properties of Type-1 solutions

Sample no	Glycol (%)	Water (%)	S (%)	C (%)	pH (%)	Viscosity (cP)	Surface Tension (mN/m)	Freezing Point (°C)
1	90	10	0	0	0	13.9	51.6	-30
2	90	9,5	0	0	0,5	13.8	51.8	-31
3	90	8	2	0	0	15.6	50.74	-30
4	90	6	0	4	0	16.5	40.1	-31
5	80	20	0	0	0	9.4	52.1	-25
6	80	19,5	0	0	0,5	10	53.5	-26
7	80	18	2	0	0	10.5	51.1	-25
8	80	16	0	4	0	14.1	40	-25
9	70	30	0	0	0	6.7	55.5	-20
10	70	29,5	0	0	0,5	7.2	54.8	-20
11	70	28	2	0	0	7.4	52	-21
12	70	26	0	4	0	8.75	39.9	-21

In Table 2.3, sample number, weight compositions of the chemicals in the solution, viscosity, surface tension and freezing point values are tabulated, respectively. Results reveal that surfactant S has no significant effect on surface tension reduction.

But, it is more effective as water ratio is was increased. But, additive S is effective on increasing viscosity especially at high glycol ratio. Additive C, which is used as corrosion inhibitor, is effective both on increasing viscosity and surface tension reduction. According to the results, additive C has more contribution on surface reduction than additive S does. No matter which glycol and water mixture is used in the experiments, additive C decreases surface tension to a certain value of 40 mN/m. Moreover, the highest viscosity in experiments is obtained with the addition of it. Additive pH has no contribution on viscosity and surface tension. But, it must be in the solution for pH stability. Since freezing point is dependent of glycol and water ratio, the other additives have no significant role.

Further investigations are performed in order to understand the changes in the solution properties when the chemicals are used together. During the investigations, different composition rates are prepared. The tests were performed at 80% ethylene glycol by weight. The results are shown in Table 2.4.

Table 2.4 Effects of chemical additives on physical properties of Type-1 solutions when they are used together

Chemical Combination	Viscosity (cP) (@ 20 °C)	Surface Tension (mN/m) (@ 25 °C)	Freezing Point (°C)
S and pH	10-15	50-53	-26
S and C	10-15	36-38	-26
pH and C	10-15	40-42	-26
S, pH and C	10-15	37-40	-26

In Table 2.4, the columns depict chemical combination, viscosity, surface tension and freezing point, respectively. Chemical combination of S, C and pH were prepared at different weight ratios. In the results, it is seen that for all combinations viscosity varies between 10 and 15 cP. However, desired surface tension is obtained by addition of additive C. In addition to this, if additives S and C are used together, lower surface tension is obtained. With the help of the results, the final composition is decided and given in Table 2.5.

Table 2.5 The final composition of de-icing fluid by weight and its physical properties

Glycol	90%
Water	9.65%
2-Ethoxyphenol	0.1%
Potassium hydrogen phosphate trihydrate	0.2%
Tributylamine	0.05%
Viscosity	15.1 cP
Surface tension	39.1 Dynes/cm
Freezing Point	- 20 °C

Since highest viscosity is obtained at a glycol ratio of 90%, final composition was prepared at this glycol ratio. The main advantage of it is to use other chemicals at a lower ratio in order to have a viscosity around 15 cP. If final composition were prepared at a lower glycol ratio, viscosity increasing chemicals, these are additive S and C, would be used in a higher ratio.

Development of de-icing solutions was studied in detail. With the help of the studies, it can be concluded that these solutions can be prepared at different chemical ratios that satisfy desired physical properties.

2.3 Development of anti-icing solutions

As mentioned before, the main differences between de-icing and anti-icing solutions are higher viscosity and shear thinning tendency that the anti-icing solutions have. Many different types of polymers were used in order to obtain these properties. A detailed analysis was performed by changing the polymer ratio, glycol/water mixture ratio and pH value of the solution. In this thesis, only the result that were obtained by using the polymer, slightly crosslinked hydrophobically modified polyacrylic acids (HMPA), will be discussed.

2.3.1 Polymer concentration effect

In the following Figures (2.1-2.3), viscosity behavior of the HMPA aqueous solutions in increasing polymer concentration are shown. They were obtained at 20°C.

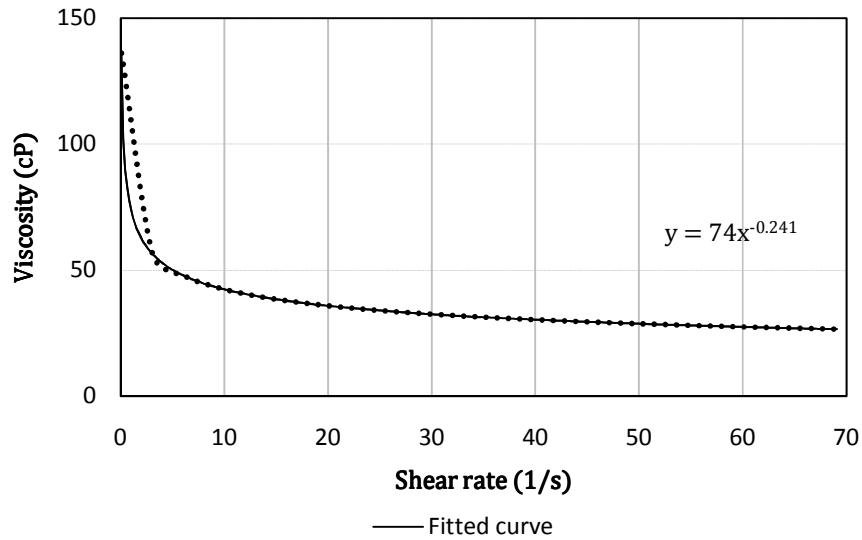


Figure 1.1 Rheological behavior of 1% of HMPA solutions by weight

The Figures (2.1-2.3) show that as polymer concentration increases both viscosity at low shear rates and shear thinning tendency increases. In addition to this, as it is seen in Figure 2.2 and Figure 2.3, 2% of HMPA solution and 4% of HMPA solution have approximately similar viscosity values at 50 1/s of shear rate. However, the pH values of all prepared solutions were around 3-3.5 which is not appropriate for material compatibility. In order to overcome this, NaOH, which increases the pH value to basic side (between 7 and 14), was added to the solution. After addition of required NaOH in order to adjust the pH value around 7, gel formation was observed and viscosity was immeasurable. After these observations, it was concluded that solutions should be prepared at lower polymer ratios and effect of pH should be carefully investigated.

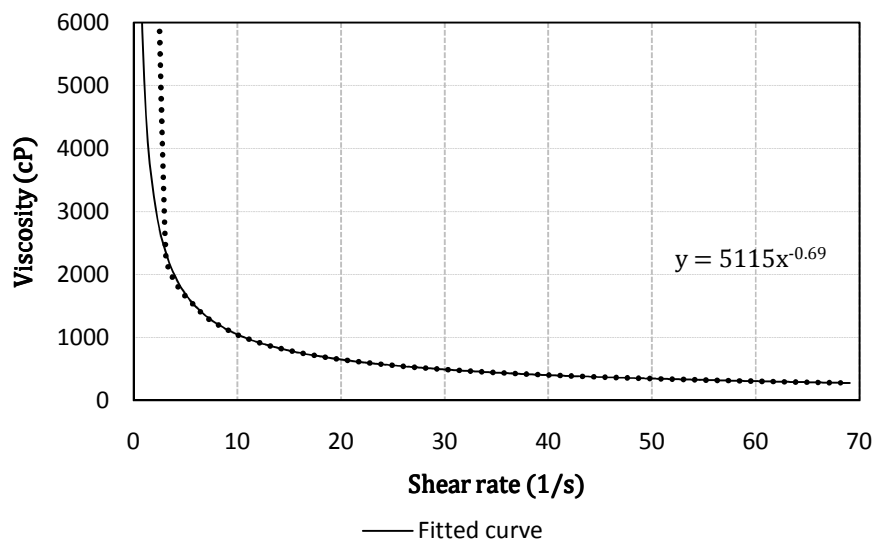


Figure 2.2 Rheological behavior of 2% wt of HMPA solutions

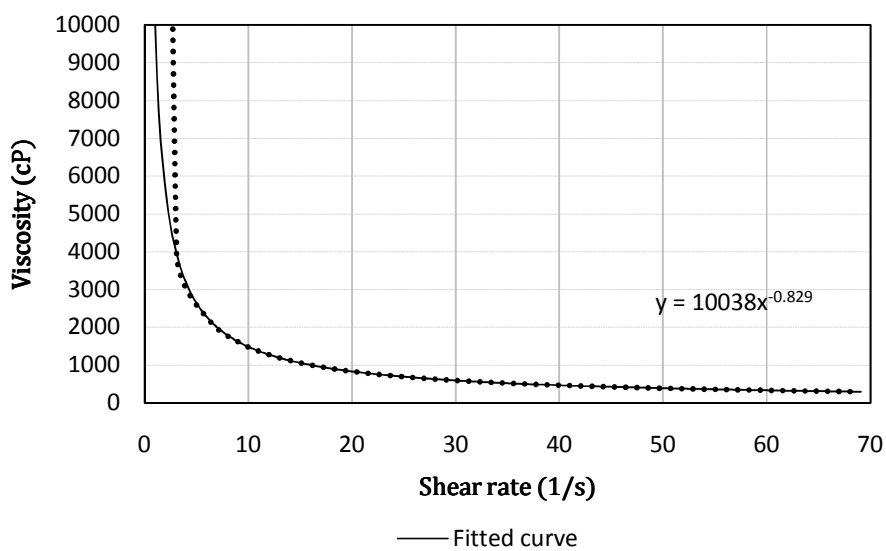


Figure 2.3 Rheological behavior of 4% wt of HMPA solutions

2.3.2 pH effect

In order to investigate the effect of pH value on solution viscosities, a lot of solutions were prepared at different polymer ratios especially around 0% and 0.25% polymer ratio by

weight. 0.075% of HPMA polymer solution was chosen in order to demonstrate the pH effect.

Dramatical dependence of viscosity to the pH value is seen in Figure 2.4. The variation of viscosity is seen especially around pH value of 6. Even a small deviation the from this value results in a sharp decrease in viscosity.

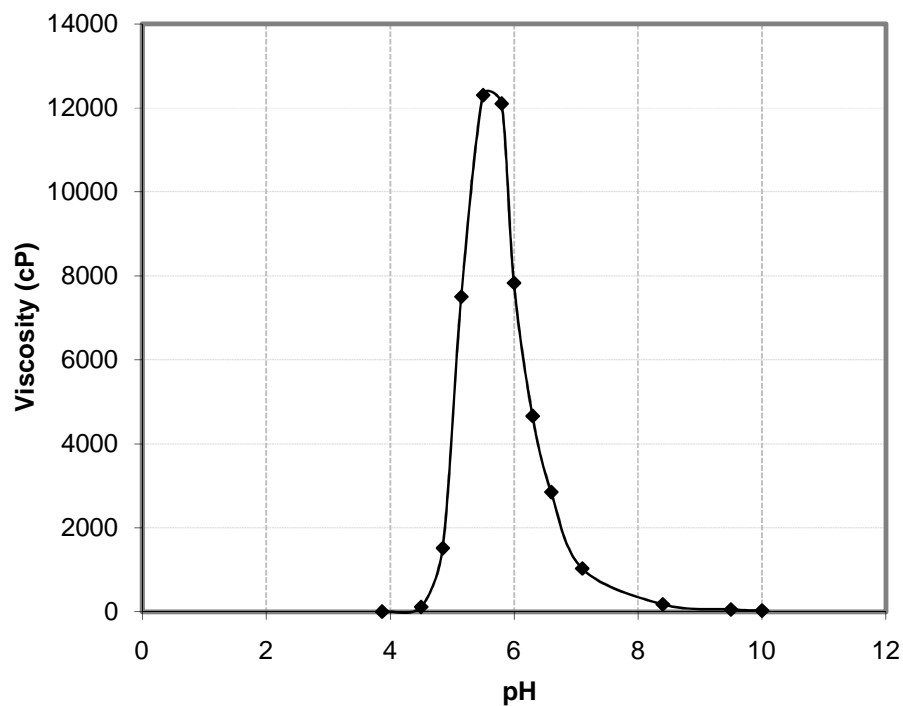


Figure 2.4 The change of zero shear viscosity of the 0.075 wt % HMPA solutions composed of 50 % water and 50 % glycol with pH

2.3.3 Glycol-water concentration effect

As discussed in development of de-icing solution part, glycol-water concentration has different rheological behaviors at different weight ratios. In this part, glycol ratio is varied from 70% to 50%. Further decrease in weight ratio of glycol is not needed because freezing

point of the solution that is prepared with these lower ratios is not in the desired range. The effect of glycol-water solution is seen at same pH value in Figure 2.5.

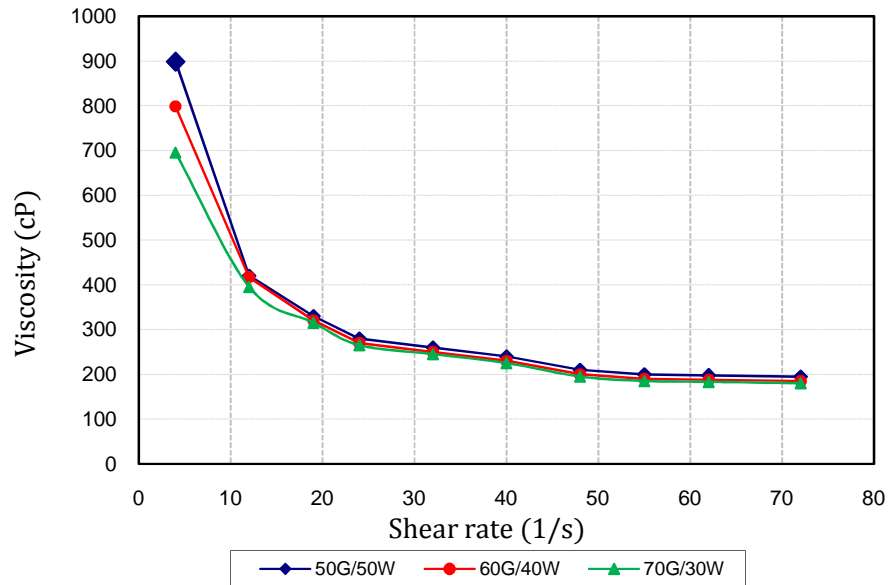


Figure 2.5 The rheological behavior of HMPA solutions at 0.064 wt % concentration with different glycol-water content.

As it is seen in Figure 2.5, when water content in the solution increases viscosity of the solution at low shear rates increases. In addition to this, it is interesting to see that at higher shear rates viscosity values of the solutions are very close to each other.

2.3.4 Surfactant effect

In de-icing and anti-icing solutions, surfactants are used in order to decrease the surface tension. During the experimental work, it was found out that surfactants are effective not only for decreasing surface tension but also modifying viscosity of solution. These effects can be visualized in Figure 2.6 and Figure 2.7.

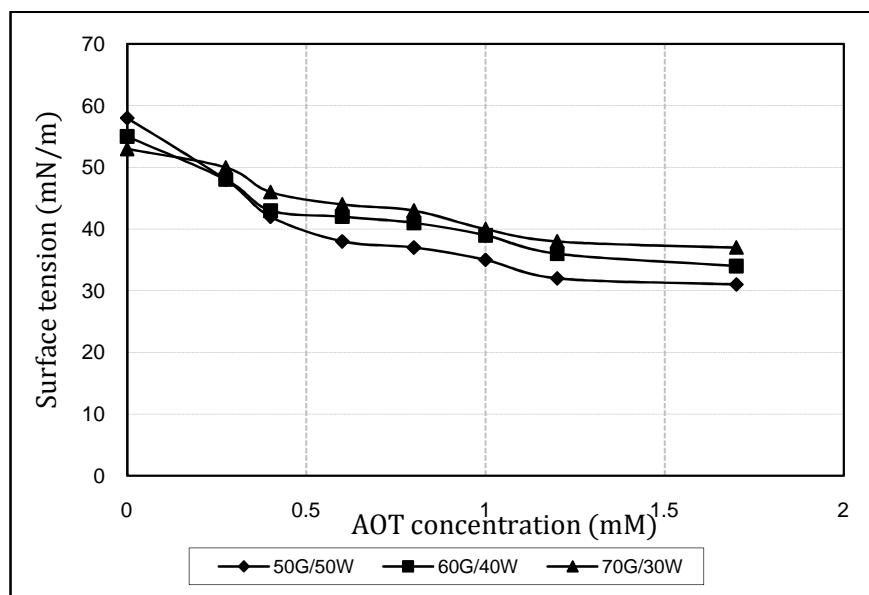


Figure 2.6 The surface tension change of HMPA solution (0.067 wt %) with addition of AOT

In Figure 2.6, the effect of AOT, 2-ethyl hexyl sulfosuccinate on the surface tension at different glycol/water concentration can be seen. In the above Figure mM defines number of moles in per unit volume of the solution. As the concentration of AOT increases, the surface tension of the solution decreases.

In Figure 2.7, the effect of AOT on the viscosity is shown. When, the concentration of AOT increases, the viscosity of the solution at low shear rates increases, except for 0.052 mM. This result shows that there is a critical value of surfactant ratio in solution beyond which viscosity at low shear rates decreases. Moreover, it can be easily stated that as shear rate increases, viscosity values of the solutions become similar.

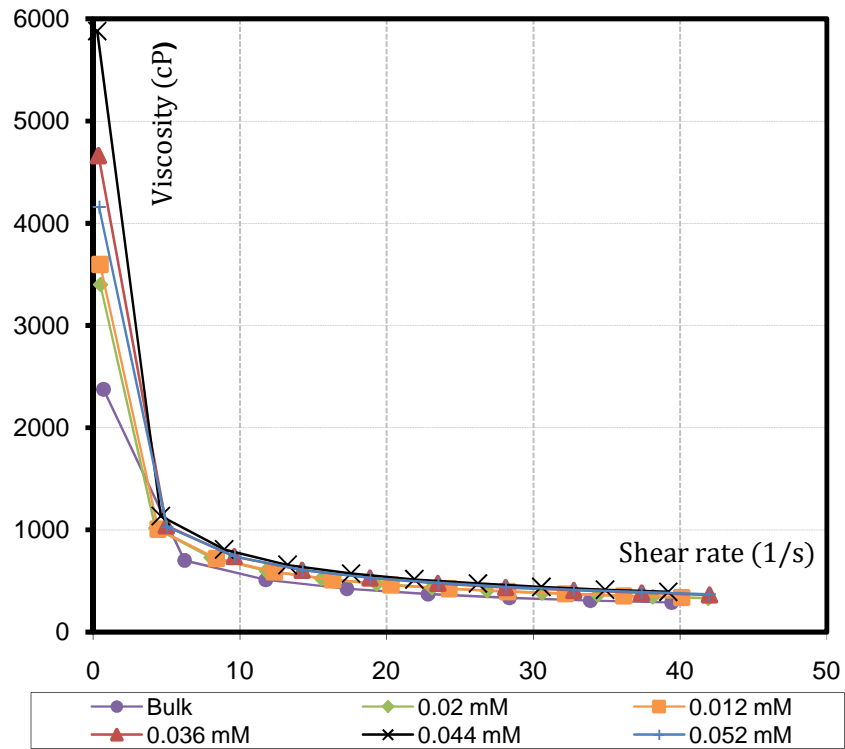


Figure 2.7 The viscosity change of HMPA solution (0.067 wt %) with addition of AOT

In this thesis, the effects of ratio of chemical additives, such as glycol/water, polymer and surfactant on the solution properties were discussed. During the investigations of these additives, different chemicals have been used. However, in this thesis the best results of the experimental works were declared. The detailed analysis of chemical additives and tests related with stability, temperature dependence, corrosion and freezing point can be found in Barış Erdoğan's M.S. thesis [19].

CHAPTER 3

MATHEMATICAL MODEL AND SOLUTION METHOD FOR THE LINEAR STABILITY ANALYSIS OF TWO-LAYER FLOWS

3.1 Objective

Another objective of this thesis is to study the behavior of the de-icing and anti-icing solutions when it is sheared by air flow. As it is mentioned in introduction part, de-icing and anti-icing solutions disturb the air flow on wings. In order to decrease this effect, solutions must flow-off as early as possible. Since experimental study requires expensive equipment, the behavior of de-icing and anti-icing solutions were tried to be estimated with a simulation. The code that was used for simulation was developed during the Ph. D. studies of Serkan Özgen [40]. In the code, minor changes were made. This chapter is devoted to mathematical model and solution method for two layer flows that is not only related to de-icing and anti-icing effects on aircraft, but also related to polymer and coating process, oceanography and cooling systems.

3.2 Introduction

In nature, there are two types of viscous fluid motions, namely laminar and turbulent. Mostly, the fluids flow with turbulent motion, except at low Reynolds numbers. However, if the disturbances are kept small, some types of fluids can be kept in laminar motion. The stability of the flow at these small disturbances is the problem of hydrodynamic stability. In order to solve the problem of hydrodynamic stability, solution of non-linear partial differential equations should be followed. Fortunately, for small disturbances the equations may be linearized. With the encouragement of Reynolds' experimental results [20], Orr (1907) [21] and Sommerfeld (1908) [22] derived an equation, known as the Orr-Sommerfeld equation, for small, wave-like disturbances and parallel flows. Early solution predictions for this equation caused to obtain results that are quite different from the

experimental results. However, the problem was overcome by Schubauer and Skramstad (1943), who obtained the waves predicted by Heisenberg and Tollmien. This mode is defined as Tollmien-Schlichting mode (TS mode) [23]. The natural evolution from laminar to turbulent flow is shown in Figure 3.1.

In this content, the location where the unstable formations are observed is important. At a certain Reynolds number, destabilizing forces are dominant and lead to instability. This Reynolds number is defined as critical Reynolds number. In Figure 3.1, critical Reynolds number is defined as the Reynolds number at transition from region A to region B.

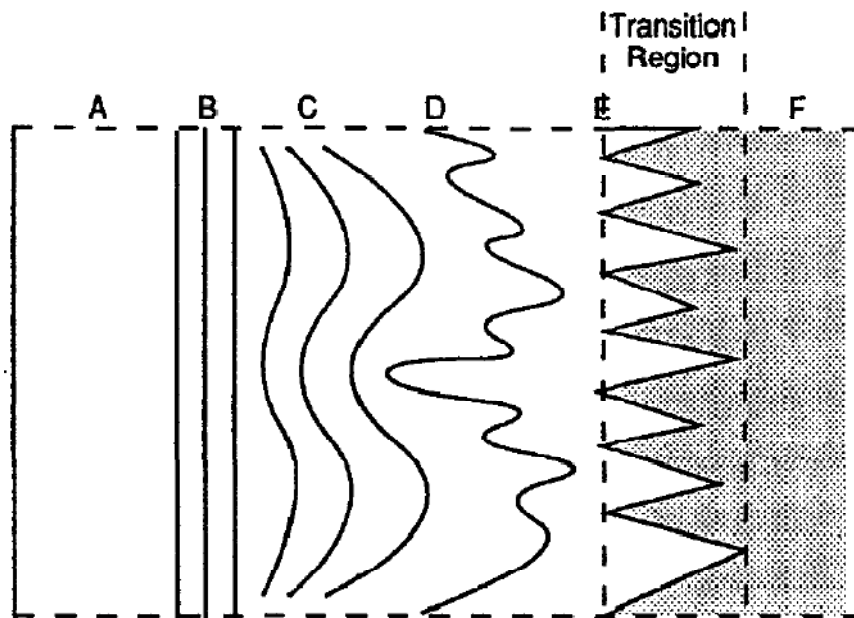


Figure 3.1 Sketch of laminar-turbulent transition [24]

In this Figure, the parts that are defined with capital letters are:

- A) Laminar flow,
- B) Unstable Tollmien-Schlichting waves,
- C) 3-D waves and vortex formation,
- D) Vortex decay,

E) Formation of turbulent spots,

F) Fully Turbulent flow.

Stability of two layer flow systems is widely dealt with due to its many applications in industry. Therefore, scientists immediately focused on this subject after the improvement in hydrodynamic stability theory.

Cohen and Hanratty [25] state that there is a critical wind velocity above which leads to 2-D waves at the interface. In their experiments, they have found out that critical wind speed increases with decreasing liquid height and increasing the shearing fluid viscosity. The disturbances at the interface do not receive their energy from the liquid, because wave velocity at the interface is always greater than the average velocity of the liquid. From the results of the experiments, they have shown that the wave at the interface gains its energy from the pressure and shear stress variations at the interface. Moreover, due to very small viscosity of air, the shear stress variations are less crucial compared to the pressure variation, except for very thin film thickness.

In one of the primary study in this area, Yih [26] found out that Couette flow, which is stable for all Reynolds numbers, and Poiseuille flow, which is unstable for large Reynolds numbers, are unstable at any Reynolds number if there is an existence of viscosity stratification. In his long wave limit analysis, he concluded that there is another mode due to the viscosity stratification apart from TS mode, which is defined as hard mode and is obtained by usual linear stability theory. The additional mode is called as Yih mode (soft mode).

Blennerhassett [27] investigated the problem both by using long wave limit analysis as Yih did, and for slow basic flow that means low Reynolds number. In his numerical work, the increase of the thickness of the upper fluid, which is air, causes an increase in critical Reynolds number and a decrease in shear stress at the interface.

Hooper and Boyd [28] approached the problem in a different manner. Contrary to the previous studies, their purpose was to study the instability problem due to viscosity stratification in the absence of rigid boundary by using short wave limit analysis. It is interesting that, they found out the short wave instability mode that is observed at equal density and in the absence of surface tension. The mode is unstable for all values of viscosity ratio, except 1. Moreover, they extended their work by investigating the effect of

density ratio and surface tension. It is found that surface tension is always stabilizing whereas; density ratio has stabilizing influence when its value is less than square of viscosity ratio.

In the experimental work of Hanratty [29], it is found that the liquids that are used instead of water, which have higher viscosity, have more stable 2-D waves than water. Yiantsios and Higgins [30] extended the study of Yih by investigating the thickness and density ratio effect on the stability problem. They obtained the critical wavelengths for different values of above parameters for hard and soft modes.

In the theoretical-experimental study of Ludwig and Hornung [31], laminar and turbulent velocity profiles were used for the upper fluid. In the experiments, disturbances were observed at lower wave numbers for the turbulent velocity profile. Moreover, their theoretical study agrees better with experimental results for laminar velocity profile.

Yih [32] analysed the wave formation on a liquid layer by using a de-icing solution, which is similar to present study. But in his study, the long wave limit restriction was not used. In his work, he calculated the critical wavenumber value for a commercially available de-icing solution both numerically and experimentally. The results that he obtained were at the same order of magnitude.

Miesen and Boersma [33] analyzed the instabilities over a thin layer flow that is disturbed by a turbulent boundary layer. They applied their work to a special case that is very beneficial for comparison with the results of present study.

In the study of Timoshin [34], he performed a parametric study for the two fluids flow system and found out the growth rate of the Ludwig and Hornung's experimental study by using long wave analysis. In his paper he states that, increase in film viscosity causes maximum growth rate to be observed at shorter waves.

In the work of Pelekasis and Tsamopoulos [35], they mainly concentrated on the gravity and surface tension effects on the neutral stability modes. They stated that as surface tension effect increases growth rates of the unstable waves decrease. In addition to this, as the gravity effect increases, the growth rate also decreases and for a certain value of gravity Yih mode is stabilized.

In the study of Özgen et al [36], neutral stability curves and amplification factors were obtained at different viscosity and density ratios, surface tension, gravity and power law index values for low, moderate and high wave numbers by using laminar boundary layer. Moreover, the turbulent velocity profile that they used for the shearing fluid is in agreement with experimental, theoretical and numerical work reported in the literature.

In another study of Özgen et al [37], details and results of analysis of wave formation and wave characteristic on a thin layer de-icing and anti-icing solutions that was deposited on the lower wall of the wind tunnel and was sheared by a turbulent air flow were investigated. Results of their experimental and numerical study are in good agreement especially for solutions that are thicker than 1 mm.

Sahu et al [38] obtained the Orr-Sommerfeld equations for Herchel-Bulkley fluids and investigated the effect of flow index and yield stress on stability. They concluded that a decrease in flow index, which causes an increase in shear-thinning tendency, has stabilizing effect for thicker Herchel-Bulkley fluids. For thinner fluids, the effect is vice versa. However, they state that for thinner fluids, dependency of the growth rate on the flow index is less. Higher yield stress is stabilizing for thinner fluids but destabilizing for thicker fluids. These mentioned results are valid for the interfacial mode (Yih mode). For TS mode, increase in shear tendency in shear index is stabilizing for all thickness and it is stated that as the fluid becomes thicker, the shear index effect becomes more crucial for stability analysis. For the same mode, it has been found out that higher yield stress is destabilizing for all fluid thickness.

Özgen [39] studied the details of the mode coalescence phenomenon in a two-layer flow stability problem. In his study, it is stated that coalescence is observed when sheared liquid thickness is sufficiently large. At high sheared liquid thickness, a composite mode that has the characteristics of TS mode at moderate wave numbers and Yih mode at low and high wave numbers. According to the results of thickness of lower fluid and surface tension variation, composite mode has more resemblance to Yih mode.

3.3 Derivations of the Orr-Sommerfeld equation

2-D Navier-Stokes and continuity equations for incompressible flows are used in order to define the motion of the fluids:

x-momentum equation:

$$\frac{\partial u^*}{\partial t^*} + u^* \frac{\partial u^*}{\partial x^*} + v^* \frac{\partial u^*}{\partial y^*} = -\frac{1}{\rho^*} \frac{\partial p^*}{\partial x^*} + \frac{1}{\rho^*} \left[\frac{\partial \sigma_{xx}^*}{\partial x^*} + \frac{\partial \tau_{yx}^*}{\partial y^*} \right], \quad (3.1)$$

y-momentum equation:

$$\frac{\partial v^*}{\partial t^*} + u^* \frac{\partial v^*}{\partial x^*} + v^* \frac{\partial v^*}{\partial y^*} = -\frac{1}{\rho^*} \frac{\partial p^*}{\partial y^*} + \frac{1}{\rho^*} \left[\frac{\partial \sigma_{yy}^*}{\partial y^*} + \frac{\partial \tau_{xy}^*}{\partial x^*} \right] - g^*, \quad (3.2)$$

Continuity Equation:

$$\frac{\partial u^*}{\partial x^*} + \frac{\partial v^*}{\partial y^*} = 0. \quad (3.3)$$

The equations of shear and normal stresses are defined as follows:

Shear stress equation:

$$\tau_{xy}^* = \tau_{yx}^* = k^* \left| 2 \left[\left(\frac{\partial u^*}{\partial x^*} \right)^2 + \left(\frac{\partial v^*}{\partial y^*} \right)^2 \right] + \left(\frac{\partial u^*}{\partial y^*} + \frac{\partial v^*}{\partial x^*} \right)^2 \right|^{\frac{n-1}{2}} \left[\frac{\partial u^*}{\partial y^*} + \frac{\partial v^*}{\partial x^*} \right], \quad (3.4)$$

Normal stress equations:

$$\sigma_{xx}^* = k^* \left| 2 \left[\left(\frac{\partial u^*}{\partial x^*} \right)^2 + \left(\frac{\partial v^*}{\partial y^*} \right)^2 \right] + \left(\frac{\partial u^*}{\partial y^*} + \frac{\partial v^*}{\partial x^*} \right)^2 \right|^{\frac{n-1}{2}} \left[2 \frac{\partial u^*}{\partial x^*} \right], \quad (3.5)$$

$$\sigma_{yy}^* = k^* \left| 2 \left[\left(\frac{\partial u^*}{\partial x^*} \right)^2 + \left(\frac{\partial v^*}{\partial y^*} \right)^2 \right] + \left(\frac{\partial u^*}{\partial y^*} + \frac{\partial v^*}{\partial x^*} \right)^2 \right|^{\frac{n-1}{2}} \left[2 \frac{\partial v^*}{\partial y^*} \right]. \quad (3.6)$$

In above equations, "*" denotes the dimensional quantities. x^* and y^* are the streamwise and normal coordinates, respectively. u^* and v^* are the velocity components in x^* and y^* coordinates. ρ^* and g^* are the density and the gravitational acceleration. n and k^* are power law index and dimensional consistency factor for non-Newtonian fluids. Notice that $n=1$ corresponds to Newtonian fluids, where k^* simply becomes the viscosity.

3.3.1 Method of small disturbances

In small disturbance theory, each flow property has a steady flow component and an unsteady fluctuating component. Since the two-dimensional disturbances cause earlier

transition compared to three dimensional disturbances according to the Squire's theorem, they are defined as a function of x and y , only:

$$u^*(x^*, y^*, t^*) = U^*(x^*, y^*) + \hat{u}^*(x^*, y^*, t^*), \quad (3.7)$$

$$v^*(x^*, y^*, t^*) = V^*(x^*, y^*) + \hat{v}^*(x^*, y^*, t^*), \quad (3.8)$$

$$p^*(x^*, y^*, t^*) = P^*(x^*, y^*) + \hat{p}^*(x^*, y^*, t^*). \quad (3.9)$$

In above equations, U^* , V^* and P^* define the steady flow properties. " $\hat{}$ " symbol defines the disturbances, while \hat{u} , \hat{v} and \hat{p} are disturbance components of velocity and pressure, respectively.

The unsteady fluctuating terms are small. Therefore, product of these terms and/or their derivatives are neglected during the rearrangement of the equations. Since the flow is assumed to be parallel flow, $U^* = U^*(y)$ and $V^* = 0$. With these assumptions, equations (3.7-3.9) are substituted into equations (3.1-3.6); the momentum and continuity equations take the form:

$$\begin{aligned} \frac{\partial \hat{u}^*}{\partial t^*} + U^* \frac{\partial \hat{u}^*}{\partial x^*} + \hat{v}^* \frac{\partial U^*}{\partial y^*} = & -\frac{1}{\rho^*} \left(\frac{\partial P^*}{\partial x^*} + \frac{\partial \hat{p}^*}{\partial x^*} \right) + \frac{k^*}{\rho^*} \frac{\partial}{\partial x^*} \left[\left| \frac{\partial U^*}{\partial y^*} + \frac{\partial \hat{u}^*}{\partial y^*} + \frac{\partial \hat{v}^*}{\partial x^*} \right|^{n-1} \left(2 \frac{\partial \hat{u}^*}{\partial x^*} \right) \right] \\ & + \frac{k^*}{\rho^*} \frac{\partial}{\partial y^*} \left[\left| \frac{\partial U^*}{\partial y^*} + \frac{\partial \hat{u}^*}{\partial y^*} + \frac{\partial \hat{v}^*}{\partial x^*} \right|^n \right], \end{aligned} \quad (3.10)$$

$$\begin{aligned} \frac{\partial \hat{v}^*}{\partial t^*} + U^* \frac{\partial \hat{v}^*}{\partial x^*} = & -\frac{1}{\rho^*} \left(\frac{\partial P^*}{\partial y^*} + \frac{\partial \hat{p}^*}{\partial y^*} \right) + \frac{k^*}{\rho^*} \frac{\partial}{\partial y^*} \left[\left| \frac{\partial U^*}{\partial y^*} + \frac{\partial \hat{u}^*}{\partial y^*} + \frac{\partial \hat{v}^*}{\partial x^*} \right|^{n-1} \left(2 \frac{\partial \hat{v}^*}{\partial y^*} \right) \right] \\ & + \frac{k^*}{\rho^*} \frac{\partial}{\partial x^*} \left[\left| \frac{\partial U^*}{\partial y^*} + \frac{\partial \hat{u}^*}{\partial y^*} + \frac{\partial \hat{v}^*}{\partial x^*} \right|^n \right] - g^*, \end{aligned} \quad (3.11)$$

$$\frac{\partial \hat{u}^*}{\partial x^*} + \frac{\partial \hat{v}^*}{\partial y^*} = 0. \quad (3.12)$$

$\frac{\partial U^*}{\partial y^*}$ term in $\left[\frac{\partial U^*}{\partial y^*} + \frac{\partial \hat{u}^*}{\partial y^*} + \frac{\partial \hat{v}^*}{\partial x^*} \right]^n$ and $\left[\frac{\partial U^*}{\partial y^*} + \frac{\partial \hat{u}^*}{\partial y^*} + \frac{\partial \hat{v}^*}{\partial x^*} \right]^{n-1}$ in (3.10) and (3.11) is

greater than other terms in above equations; the binomial distribution can be used in order to expand these terms. These are:

$$\left[\frac{\partial U^*}{\partial y^*} + \frac{\partial \hat{u}^*}{\partial y^*} + \frac{\partial \hat{v}^*}{\partial x^*} \right]^n \approx \left| \frac{\partial U^*}{\partial y^*} \right|^n + n \left| \frac{\partial U^*}{\partial y^*} \right|^{n-1} \frac{\partial \hat{u}^*}{\partial y^*} + n \left| \frac{\partial U^*}{\partial y^*} \right|^{n-1} \frac{\partial \hat{v}^*}{\partial x^*}, \quad (3.13)$$

$$\left[\frac{\partial U^*}{\partial y^*} + \frac{\partial \hat{u}^*}{\partial y^*} + \frac{\partial \hat{v}^*}{\partial x^*} \right]^{n-1} \approx \left| \frac{\partial U^*}{\partial y^*} \right|^{n-1} + (n-1) \left| \frac{\partial U^*}{\partial y^*} \right|^{n-2} \frac{\partial \hat{u}^*}{\partial y^*} + (n-1) \left| \frac{\partial U^*}{\partial y^*} \right|^{n-2} \frac{\partial \hat{v}^*}{\partial x^*}. \quad (3.14)$$

If equations (3.13-3.14) are substituted into equations (3.10-3.11) and the derivatives are taken, the equations shown below are obtained:

$$\begin{aligned} \frac{\partial \hat{u}^*}{\partial t^*} + U^* \frac{\partial \hat{u}^*}{\partial x^*} + \hat{v}^* \frac{\partial U^*}{\partial y^*} = & -\frac{1}{\rho^*} \left(\frac{\partial P^*}{\partial x^*} + \frac{\partial \hat{p}^*}{\partial x^*} \right) + \frac{k^* n(n-1)}{\rho^*} \left| \frac{\partial U^*}{\partial y^*} \right|^{n-2} \left[\frac{\partial^2 U^*}{\partial y^{*2}} \left(\frac{\partial \hat{u}^*}{\partial y^*} + \frac{\partial \hat{v}^*}{\partial x^*} \right) \right] \\ & + \frac{k^*}{\rho^*} \left| \frac{\partial U^*}{\partial y^*} \right|^{n-1} \left[2 \frac{\partial^2 \hat{u}^*}{\partial x^{*2}} + n \frac{\partial^2 \hat{u}^*}{\partial y^{*2}} + n \frac{\partial^2 \hat{v}^*}{\partial x^* \partial y^*} + n \frac{\partial^2 U^*}{\partial y^{*2}} \right], \end{aligned} \quad (3.15)$$

$$\begin{aligned} \frac{\partial \hat{v}^*}{\partial t^*} + U^* \frac{\partial \hat{v}^*}{\partial x^*} = & -\frac{1}{\rho^*} \left(\frac{\partial P^*}{\partial y^*} + \frac{\partial \hat{p}^*}{\partial y^*} \right) + \frac{k^* 2(n-1)}{\rho^*} \left| \frac{\partial U^*}{\partial y^*} \right|^{n-2} \left[\frac{\partial^2 U^*}{\partial y^{*2}} \left(\frac{\partial \hat{v}^*}{\partial y^*} \right) \right] \\ & + \frac{k^*}{\rho^*} \left| \frac{\partial U^*}{\partial y^*} \right|^{n-1} \left[n \frac{\partial^2 \hat{v}^*}{\partial x^{*2}} + 2 \frac{\partial^2 \hat{v}^*}{\partial y^{*2}} + n \frac{\partial^2 \hat{u}^*}{\partial x^* \partial y^*} \right] - g^*. \end{aligned} \quad (3.16)$$

In the next step, nondimensionalization should be performed. These are defined as follows:

$$t = \frac{t^* U_e^*}{d^*}, x = \frac{x^*}{d^*}, y = \frac{y^*}{d^*}, \hat{u} = \frac{\hat{u}^*}{U_e^*}, \hat{v} = \frac{\hat{v}^*}{U_e^*}, \hat{p} = \frac{\hat{p}^*}{\rho^* U_e^{*2}}, Re = \frac{\rho^* U_e^* d^*}{k^*} \quad (3.17)$$

In above steps, d^* and U_e^* values the characteristic length and characteristic boundary layer limiting freestream velocity that are defined according to the the upper fluid velocity profile in section 3.4.1.

After the terms containing mean flow quantities only are removed from the above equations and they become:

$$\begin{aligned} \frac{\partial \hat{u}}{\partial t} + U \frac{\partial \hat{u}}{\partial x} + \hat{v} \frac{\partial U}{\partial y} = & -\frac{\partial \hat{p}}{\partial x} + \frac{n(n-1)}{Re} \left[\left| \frac{\partial U}{\partial y} \right|^{n-2} \frac{\partial^2 U}{\partial y^2} \left(\frac{\partial \hat{u}}{\partial y} + \frac{\partial \hat{v}}{\partial x} \right) \right] \\ & + \frac{1}{Re} \left| \frac{\partial U}{\partial y} \right|^{n-1} \left[2 \frac{\partial^2 \hat{u}}{\partial x^2} + n \frac{\partial^2 \hat{u}}{\partial y^2} + n \frac{\partial^2 \hat{v}}{\partial x \partial y} \right], \end{aligned} \quad (3.18)$$

$$\begin{aligned} \frac{\partial \hat{v}}{\partial t} + U \frac{\partial \hat{v}}{\partial x} = -\frac{\partial \hat{p}}{\partial y} + \frac{2(n-1)}{\text{Re}} \left[\left| \frac{\partial U}{\partial y} \right|^{n-2} \frac{\partial^2 U}{\partial y^2} \frac{\partial \hat{v}}{\partial y} \right] \\ + \frac{1}{\text{Re}} \left| \frac{\partial U}{\partial y} \right|^{n-1} \left[n \frac{\partial^2 \hat{v}}{\partial x^2} + 2 \frac{\partial^2 \hat{v}}{\partial y^2} + n \frac{\partial^2 \hat{u}}{\partial x \partial y} \right], \end{aligned} \quad (3.19)$$

$$\frac{\partial \hat{u}}{\partial x} + \frac{\partial \hat{v}}{\partial y} = 0. \quad (3.20)$$

In this study temporal analysis is used. In temporal theory, wave number α is real, and phase velocity $c = c_r + ic_i$ is complex. c_r is phase speed and c_i is temporal amplification factor. The disturbance stream function is defined as follows:

$$\Phi(x, y, t) = \chi(y) e^{\alpha c_i t} e^{i\alpha(x - c_r t)} \quad (3.21)$$

In the temporal analysis, the solution only oscillates in space, but is allowed to grow and decay in time. Temporal amplification factor is:

$$\sigma = \alpha c_i. \quad (3.22)$$

Temporal amplification factor, c_i , yields the following configurations:

$c_i < 0 \rightarrow$ the wave is stable,

$c_i = 0 \rightarrow$ the wave is neutrally stable,

$c_i > 0 \rightarrow$ the wave is unstable.

The numerical methods, which are for asymptotic solutions for the Orr-Sommerfeld equations, are easier to find especially for large Reynolds numbers in temporal analysis. Therefore, in this study, temporal analysis method is used.

3.3.2 Method of normal modes

In section 3.3.1, infinitely small perturbations are introduced to the primary flow. These small disturbances are assumed to be periodic in x direction according to the normal modes assumptions. The disturbance function is defined with the help of temporal approach described above, as follows:

$$\Phi(x, y, t) = \chi(y) e^{i\alpha(x - ct)} \quad (3.23)$$

In above formulation, χ is the disturbance amplitude function, $\alpha = 2\pi/\lambda$ (λ is the wavelength) is wave number and c is phase velocity. The velocity and pressure fluctuations are defined as follows:

$$\hat{u} = \frac{\partial \Phi}{\partial y} = \chi'(y)e^{i\alpha(x-ct)}, \quad (3.24)$$

$$\hat{v} = -\frac{\partial \Phi}{\partial x} = -i\alpha\chi(y)e^{i\alpha(x-ct)}, \quad (3.25)$$

$$\hat{p} = \lambda(y)e^{i\alpha(x-ct)}. \quad (3.26)$$

If these fluctuations are substituted into equations (3.18-3.20), equations (3.27-3.29) are obtained:

$$-(U - c)\chi' + \chi U' = \lambda - \frac{|U'|^{n-2}}{i\alpha Re} [n(n-1)U''(\chi'' + \alpha^2\chi)] - \frac{|U'|^{n-1}}{i\alpha Re} [(n-2)\alpha^2\chi' + n\chi'''], \quad (3.27)$$

$$(U - c)\alpha^2\chi = -\lambda' - \frac{|U'|^{n-2}}{i\alpha Re} [2(n-1)\alpha^2U''\chi'] + \frac{|U'|^{n-1}}{i\alpha Re} [(n-2)\alpha^2\chi'' + n\alpha^4\chi], \quad (3.28)$$

$$i\alpha\chi' - i\alpha\chi' = 0. \quad (3.29)$$

In above equations, the primes (') denote differentiation with respect to non-dimensional y -distance.

In equation 3.29, it is seen that perturbations obey the continuity equation. In order to eliminate the pressure terms, derivative of equation 3.27 is taken with respect to y and the sum of the new equation and equation 3.28 results in the following:

$$\begin{aligned} (U - c)(\chi'' - \alpha^2\chi) - U''\chi &= \frac{|U'|^{n-3}}{i\alpha Re} \{(U')^2 n(\chi'''' - 2\alpha^2\chi'' + 2\alpha^4\chi) + (n-1)\{2nU'U''\chi'' \\ &+ [4\alpha^2(U')^2 + nU'U'''' + n(n-2)((U'')^2)]\chi'' \\ &+ 2(n-2)\alpha^2U'U''\chi' + n\alpha^2[U'U'''' + (n-2)(U'')^2]\chi\} \end{aligned} \quad (3.30)$$

This is the Orr-Sommerfeld equation for power-law fluids. According to the fluid's viscosity behavior and velocity profile that it has, the equation can be simplified.

In fact, the mathematical modeling of two-layer flows was derived before by Özgen [40]. Since, method of small disturbance and defining them with a function are important works in transition prediction and turbulent studies, mathematical modeling was obtained one more time in this study and compared with Özgen's results. The result obtained in this study is same to his results.

3.4 Two-layer flow

The flow geometry of the system treated in this study can be seen in Figure 3.2.

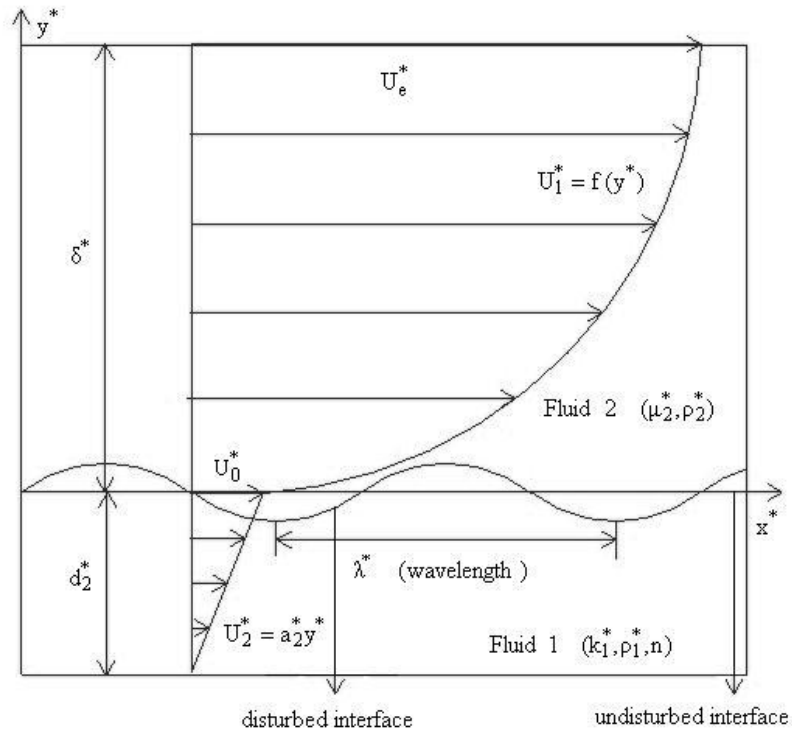


Figure 3.2 Flow system geometry

Above, the Orr-Sommerfeld equation for 2-D, incompressible fluids flows was derived. Now, the aim is to solve the stability problem of two-layer fluid flows by using the Orr-Sommerfeld equation. In this work, the lower fluid has either Newtonian or pseudoplastic

behavior with a linear velocity profile U_2 , whereas, the upper fluid is air with a laminar or turbulent boundary layer velocity profile U_1 .

The lower fluid's velocity profile is assumed to be linear, $U_2'' = U_2''' = 0$. Therefore, the Orr-Sommerfeld equation takes the following form:

$$(U_2 - c)(\chi'' - \alpha^2\chi) = \frac{ma_2^{n-1}}{i\alpha r \text{Re}} (n\chi'''' - 2(n-2)\alpha^2\chi'' + n\alpha^4\chi). \quad (3.31)$$

In above equation, $a_2 = U_0/l$, $U_0 = (a_1/m)^{1/n} \cdot l$, $m = (k_2^*/\mu_1^*)(U_e^*/d^*)^{(n-1)}$ and $l = d_2^*/d^*$. a_1 and a_2 are upper and lower fluid velocity gradients at the interface. k_2^* , n and d_2^* are the consistency factor, power law index and thickness of the lower fluid. U_0 is the velocity at the interface and U_e^* is the upper fluid freestream velocity with respect to interface. $r = \rho_2^*/\rho_1^*$ is the ratio of densities, m is the viscosity ratio and $\text{Re} = \rho_1^*U_e^*d^*/\mu_1^*$ is the Reynolds number.

The upper fluid is Newtonian ($n=1$). As a result, Orr-Sommerfeld equation becomes:

$$(U_1 - c)(\varphi'' - \alpha^2\varphi) - U_1''\varphi = \frac{1}{i\alpha \text{Re}} (\varphi'''' - 2\alpha^2\varphi'' + \alpha^4\varphi). \quad (3.32)$$

In the above equation, φ is the disturbance amplitude function for upper fluid. If the boundary and freestream conditions are investigated, at wall due to no-slip condition perturbations vanish:

$$y = -l \quad \Rightarrow \quad \chi = \chi' = 0. \quad (3.33)$$

At higher values of y , the perturbations also vanish:

$$y \rightarrow \infty \quad \Rightarrow \quad \varphi \rightarrow 0, \varphi' \rightarrow 0. \quad (3.34)$$

Moreover, at the interface, continuity of normal and streamwise velocities and continuity of shear and normal stresses should be satisfied (see Appendix A). These are shown below, respectively.

$$\varphi(0) = \chi(0), \quad (3.35)$$

$$\varphi'(0) - \chi'(0) = \frac{\varphi(0)}{c - U_0} (a_2 - a_1). \quad (3.36)$$

$$\alpha^2 \varphi(0) + \varphi''(0) = mna_2 \frac{\varphi(0)}{c - U_0} (\alpha^2 \chi(0) + \chi''(0)) \quad (3.37)$$

$$\begin{aligned} & i\alpha R((c - U_0)\varphi'(0) + a_1\varphi(0)) - (\varphi'''(0) - 3\alpha^2\varphi'(0)) + i\alpha Rr((c - U_0)\chi'(0) + a_2\chi(0)) \\ & + ma_2^{n-1}[n\chi''(0) - (4 - n)\alpha^2\chi'(0)] = i\alpha R[(r - 1)F^2 + \alpha^2 S] \varphi / \tilde{c} \end{aligned} \quad (3.38)$$

In equation 3.38, surface tension parameter, $S = T^*/\rho_1^*U_e^{*2}d^*$, and Froude number, $F = U_e^*/(g^*d^*)^{1/2}$ are defined. Surface tension coefficient T^* , and gravitational acceleration g^* , are included in these parameters, respectively.

As it is seen in Orr-Sommerfeld equations, in order to solve these equations velocity profile and its derivatives should be known. In this work two velocity profiles are used. They are laminar and turbulent velocity profiles.

3.4.1 Laminar and turbulent boundary layer

3.4.1.1 Laminar boundary layer

In order to generate laminar velocity profile Falkner-Skan equation without pressure gradient is used:

$$2f''' + ff'' = 0 \quad (3.39)$$

In above equation, $f' = U_1$. The boundary condition for the upper fluid is defined as follows:

$$f = f' = 0 \text{ at } y = 0, \quad (3.40)$$

$$f' \rightarrow 1 \text{ at } y \rightarrow \infty. \quad (3.41)$$

The velocity profile for the lower fluid is linear and defined as follows:

$$U_2 = a_2 y, \quad (3.42)$$

The boundary conditions for the lower fluids are:

$$U_2 = U_0 \text{ at } y = 0, \quad (3.43)$$

$$U_2 = 0 \text{ at } y = -1. \quad (3.44)$$

When this velocity profile is used, the Falkner-Skan length scale is used for non-dimensionalization:

$$d^* = d_1^* = \sqrt{\frac{v^* x^*}{U_e^*}}. \quad (3.45)$$

For velocities the boundary layer limiting velocity with respect to interface U_e^* , is used.

3.4.1.2 Turbulent boundary layer

In this part, turbulent velocity profile is defined in two parts. The first part is laminar viscous sublayer with a linear velocity profile that is located immediately above the interface [37]. The laminar velocity profile is defined as follows:

$$U_1^* = (u_*^2/v_1^*)y^* \quad \text{for} \quad 0 \leq y^* \leq sv_1^*/u_*. \quad (3.46)$$

In above equation, s is the extent of laminar sublayer that has a value of around 5 and 8, v_1^* is the kinematic viscosity of the upper fluid layer. u_* is the friction velocity and defined as follows:

$$u_* = \sqrt{\tau_0^*/\rho_1^*}. \quad (3.47)$$

In above equation, the shear stress at the interface is $\tau_0^* = (1/2)\rho_1^*U_e^{*2}C_f$. C_f is the skin friction coefficient and has a value of 0.02 [37].

Turbulent part is defined as follows:

$$U_1^* = ay^{*c} + b/y^{*2} + d \quad \text{for} \quad y^* \geq sv_1^*/u_*. \quad (3.48)$$

In above equation, parameters a , b and d are determined from the continuity of velocity, the first and second derivatives of velocity at $y^* = sv_1^*/u_*$, respectively. Parameter c is obtained by satisfying the freestream boundary condition. When, this boundary layer is used, non-dimensionalization is done with d_2^* for lengths and U_e^* for velocities.

3.5 Solution method

The solution method is the backward integration method [24]. The method is based on choosing the distance away from the interface so that $U(y_e) = 1$ and $U''(y_e) = 0$ and

integrating the Orr-Sommerfeld and velocity profile equations simultaneously. For integration, a fifth order accurate Runge-Kutta integrator is used. Starting values of the Orr-Sommerfeld equation is specified by using $y \rightarrow \infty$, $U(y_e) = 1$ and $U''(y_e) = 0$. If these are applied, equation 3.32 reduces to:

$$\varphi'''' - (\alpha^2 + \beta^2)\varphi'' + \alpha^2\beta^2\varphi = 0 \quad (3.49)$$

In above equation, $\beta^2 = \alpha^2 + i\alpha R(1 - c)$. Equation 3.49 has a general solution defined below:

$$\varphi = A_1 \exp(-\alpha y) + A_2 \exp(-\beta y) + A_3 \exp(\alpha y) + A_4 \exp(\beta y). \quad (3.50)$$

If equation 3.34 is applied:

$$\varphi = A_1 \exp(-\alpha y) + A_2 \exp(-\beta y), \quad (3.51)$$

is obtained. Since the equation is fourth order, two initial vectors should be specified in order to start the integration:

$$[\varphi_1, \varphi_1', \varphi_1'', \varphi_1'''] = [1, -\alpha, \alpha^2, -\alpha^3], [\varphi_2, \varphi_2', \varphi_2'', \varphi_2'''] = [1, -\beta, \beta^2, -\beta^3]. \quad (3.52)$$

However, β term includes Re. Therefore, during integration the growth of second solution is much larger which causes loss of linear dependence of two solutions. In order to prevent this Gram-Schmidt orthonormalization procedure is applied. Gram-Schmidt procedure is defined as follows:

$$R_1 = \Omega, \quad (3.53)$$

$$R_2 = \Theta - \text{proj}_{R_1} \Theta. \quad (3.54)$$

In above equations, Ω and Θ are defined as the solution vector of φ_1 and φ_2 , respectively. In equation 3.54, $\text{proj}_{R_1} \Theta$ is defined as follows:

$$\text{proj}_{R_1} \Theta = \langle R_1, \Theta \rangle \frac{R_1}{\langle R_1, R_1 \rangle}. \quad (3.55)$$

In above equation, $\langle \rangle$ defines the inner product of vectors in it. R_1 and R_2 are the new orthonormal vectors. After that, equation 3.32 is started to be integrated with these initial values towards the interface. When the solution reaches interface, Orr-Sommerfeld

equation 3.31 for lower layer is started to be used. Unfortunately, there is no reduction for this equation. It has a general solution of the form:

$$\chi = B_1\chi_1 + B_2\chi_2 + B_3\chi_3 + B_4\chi_4. \quad (3.56)$$

The starting values of the integral for lower layer cannot be obtained with a similar manner for upper layer. Therefore, four linearly independent solutions are chosen as those corresponding to an orthonormal basis of initial vectors. These are:

$$\chi_1 = [1, 0, 0, 0], \chi_2 = [0, 1, 0, 0], \chi_3 = [0, 0, 1, 0], \chi_4 = [0, 0, 0, 1] \quad (3.57)$$

However, if the boundary condition in equation 3.33 is used, first and second terms vanish. For simplicity, third and fourth terms are defined with subscripts 1 and 2, respectively. The new equation is started to be integrated from the wall to the interface. When solutions meet at interface, they should satisfy interface conditions given in equations (3.35-3.38). These condition yields a coefficient matrix shown below:

$$\begin{bmatrix} c_{11} & c_{12} & c_{13} & c_{14} \\ c_{21} & c_{22} & c_{23} & c_{24} \\ c_{31} & c_{32} & c_{33} & c_{34} \\ c_{41} & c_{42} & c_{43} & c_{44} \end{bmatrix} \begin{bmatrix} A_1 \\ A_2 \\ B_1 \\ B_2 \end{bmatrix} = \begin{bmatrix} 0 \\ 0 \\ 0 \\ 0 \end{bmatrix}. \quad (3.58)$$

The elements of above matrix are:

$$c_{11} = \phi_1 \quad (3.59)$$

$$c_{12} = \phi_2 \quad (3.60)$$

$$c_{13} = -\chi_1 \quad (3.61)$$

$$c_{14} = -\chi_2 \quad (3.62)$$

$$c_{21} = \phi_1' - \frac{\phi_1}{\bar{c}}(a_2 - a_1) \quad (3.63)$$

$$c_{22} = \phi_2' - \frac{\phi_2}{\bar{c}}(a_2 - a_1) \quad (3.64)$$

$$c_{23} = -\chi_1' \quad (3.65)$$

$$c_{24} = -\chi_2' \quad (3.66)$$

$$c_{31} = \alpha^2 \phi_1 + \phi_1'' \quad (3.67)$$

$$c_{32} = \alpha^2 \phi_2 + \phi_2'' \quad (3.68)$$

$$c_{33} = -mn\alpha_2^{n-1}(\chi_1'' + \alpha^2\chi_1) \quad (3.69)$$

$$c_{34} = -mn\alpha_2^{n-1}(\chi_2'' + \alpha^2\chi_2) \quad (3.70)$$

$$c_{41} = -i\alpha R(\tilde{c}\phi_1' + a_1\phi_1) - (\phi_1''' - 3\alpha^2\phi_1') - i\alpha R[(r-1)F^{-2} + \alpha^2S]\phi_1/\tilde{c} \quad (3.71)$$

$$c_{42} = -i\alpha R(\tilde{c}\phi_2' + a_1\phi_2) - (\phi_2''' - 3\alpha^2\phi_2') - i\alpha R[(r-1)F^{-2} + \alpha^2S]\phi_2/\tilde{c} \quad (3.72)$$

$$c_{43} = i\alpha Rr(\tilde{c}\chi_1' + a_2\chi_1) + m\alpha_2^{n-1}(n\chi_1''' - (4-n)\alpha^2\chi_1') \quad (3.73)$$

$$c_{44} = i\alpha Rr(\tilde{c}\chi_2' + a_2\chi_2) + m\alpha_2^{n-1}(n\chi_2''' - (4-n)\alpha^2\chi_2') \quad (3.74)$$

The determinant of the matrix given in equation 3.58 should vanish for a non-trivial solution for certain combinations of Re, α, c_r and c_i . In order to obtain neutral stability curves, c_i and Re values of the solution are kept constant while c_r and α are searched. In order to obtain a stability curve two starting points should be known. These points are obtained by function minimization subroutine based on simplex method [40]. Once these points are found, Newton iteration method is used in order to find the remaining points faster.

In this thesis, the only thing that was performed for the solution method is to change the function minimization method. The original code was used to have to connect to another computer in the network in order to use function minimization subroutine in Fortran Nag library. What was done in this study is to change the function minimization subroutine with subroutine in Özgen's linear stability code for single-layer flow so that the code can run independently.

CHAPTER 4

RESULTS AND DISCUSSION

4.1 Objective

The main aim in this chapter is defined in two ways. First aim is to investigate the effect of properties such as viscosity, density, thickness, surface tension, gravity and shear thinning tendency on stability characteristics of two-layer flows by a parametric study. Second one is to find the wave characteristics of developed and commercially available de-icing and anti-icing solutions and predict whether developed solutions can pass the aerodynamic acceptance test or not according to their wave characteristics. For the parametric study, upper fluid, in this study it is air, has a laminar boundary layer. For the comparison of the solutions' wave characteristics, upper fluid has a turbulent boundary layer. Before being concentrating on the details of the studies, a validation of the mathematical modeling and numerical approximation is performed for each case.

4.2 Results obtained by using laminar boundary layer

4.2.1 Validation of the method

In order to validate the numerical approximation of the procedure, a comparison is made by using the parameters that Yih [32] used in his work. The 1.1 mm thickness de-icing fluid that he used in his experiments has a viscosity of 10 Pa.s at -10°C . At this temperature air viscosity is $1.67 * 10^{-5}$ Pa.s. This yields a viscosity ratio, $m=598802$. The fluid-air density ratio is 972, where air density is 1.342 kg/m^3 . The surface tension between fluid-air is 31.3 mN/m. The freestream velocity U_e^* is 27.28 m/s. With the help of this data, the l , S , F , Re values are obtained as follows, 3.5668, 0.10127, 496 and 678, respectively. The result that is obtained by Yih is obtained by using the long wave number limit method. But, the

study of Hendrickson and Hill [41] is based on arbitrary wave number which is the method that is used in this thesis for comparison. Amplification rate for the Yih's work is obtained for TS mode by using the numerical procedure in this work and plotted in Figure 4.1.

In the results, the maximum growth rate is obtained at $\alpha=0.1506$. In the study of Hendrickson, this value was found as $\alpha=0.1402$. Yih found this value as 0.5. However, he used lower fluid's thickness for non-dimensionalization. If the Blasius length scale is used for reference length, it turns out to be 0.1402. Our result matches very well with Yih's and Hendrickson's results. Moreover, Yih states that α value should be more or less at the order of 0.2 according to the TS waves for Blasius flow. In our result the α value at maximum growth rate is 0.3342. This prediction also confirms our numerical procedure. Since Yih declared his result just with a number, there is no graph for comparison of results.

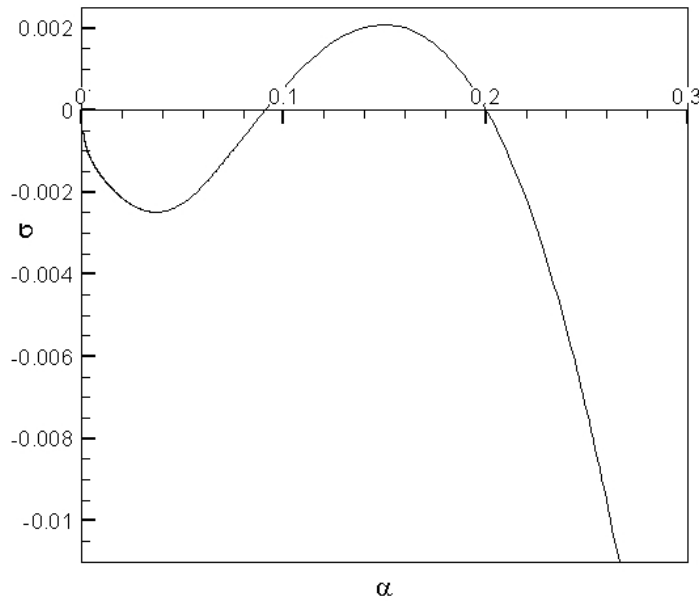


Figure 4.1 Amplification rate for Yih's case for TS mode ($m = 598802$, $r = 972$, $l = 3.5668$, $S = 0.1027$, $F = 496$, $R = 678$)

4.2.2 Parametric study

In this part the effects of physical and rheological properties on the interfacial stability will be investigated. Since some of the studies in the literature are based on interfacial (soft) mode that arises due to viscosity stratification, viscosity stratification is always considered during parametric study.

As it is seen in Figure 4.2, the thick lines describes neutral TS mode. The area in this curve is unstable, whereas remaining region is stable. In addition to this, there are two more neutral stability curves, where very short waves (high wave numbers) and long waves (low wave numbers) are observed. These are defined with thin lines. Contrary to TS mode, the area in these curves are stable, where as surrounding region is unstable.

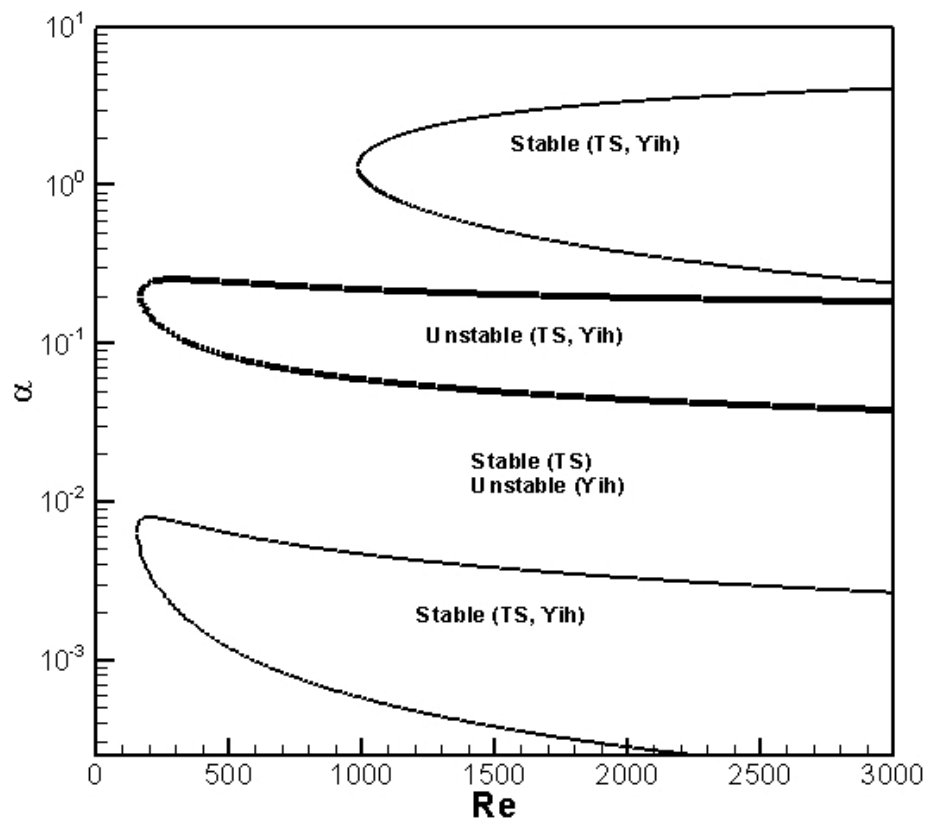


Figure 4.2 Neutral stability curves for the two instability modes ($m = 5, l = 0.5, r = 1, S = 0, F = 0$)

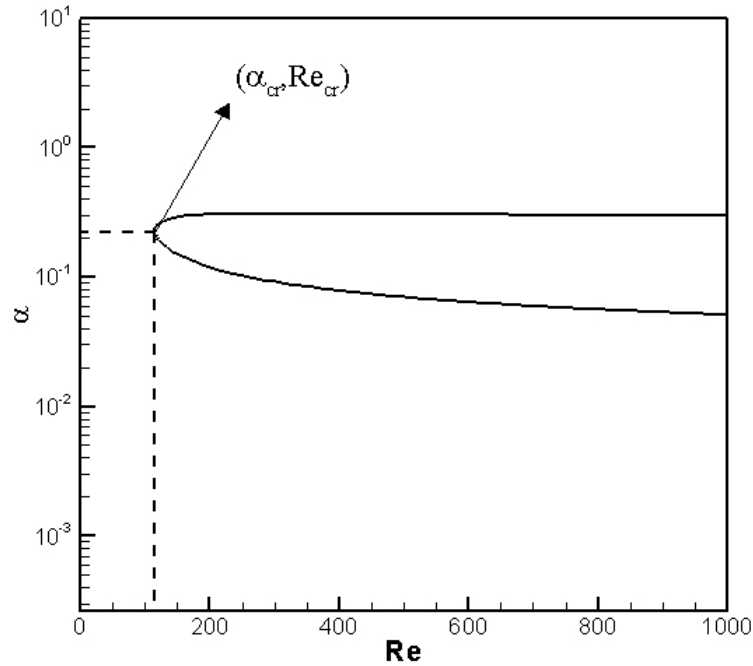


Figure 4.3 α_{cr} and Re_{cr} on TS neutral stability curve ($m = 10, l = 1, r = 1, S = 0, F = 0$)

In Figure 4.3, α_{cr} and Re_{cr} are shown on a TS neutral stability curve. The location of this point is important. Because, for Reynolds number less than Re_{cr} , flow is totally stable or unstable according to its neutral stability mode.

Since the most important parameter is viscosity, which causes two different stability modes, it is better to start with its effect. Since Figure 4.4 is a little complicated, it is better to start with low wave numbers. As it is seen, as the viscosity ratio is increased by increasing the viscosity of the lower fluid the area of the stable region is decreased. Moreover, as m is increased to 100, the stable region is not observed.

As the wave number is increased, combined modes are observed for small values of m . These combined modes are mainly due to thickness ratio of the fluids that will be explained soon. But it is a striking result that as the m value is increased the combined mode disappears and TS mode becomes the only mode that can be obtained in this wave number region.

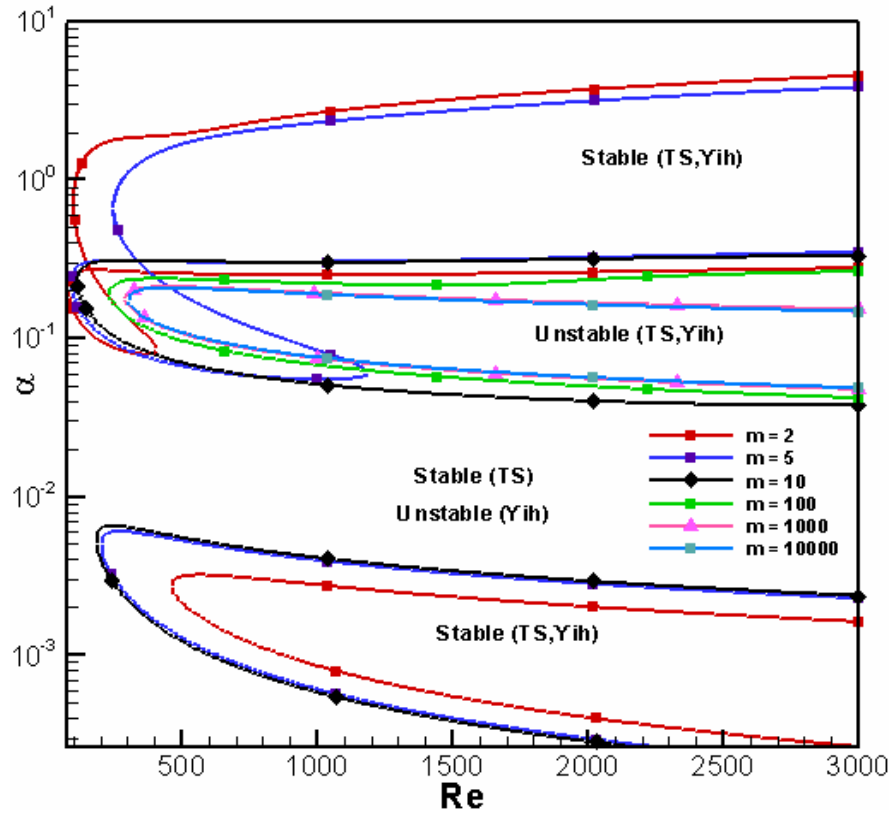


Figure 4.4 Effect of viscosity ratio m ($l = 1, r = 1, S = 0, F = 0$)

In Yih's well known study, which investigates the interfacial stability between a de-icing fluid, where $m \cong 10^6$, it is stated that the stability at the interface is interfacial stability. However, Özgen [38] states that Yih's study includes some numerical errors that causes the observed mode to be interpreted as the Yih mode. If TS mode is investigated in detail, it is seen that as m value is increased, the mode shifts to the right and unstable region decreases up to a limit. At this value due to the high value of m , the lower fluid behaves as if it is a wall. Since, there must be shear and normal stress continuity at the interface, the velocity gradient of lower fluid will be very small compared to the upper fluid's velocity gradient due to high m value. So it is concluded that the system turns out to be one-layer flow system for higher values of m .

In Figure 4.5, the effect of thickness ratio is seen. Increasing thickness ratio causes to move the interface away from the wall. For low wave numbers, as thickness ratio is increased, the stable region decreases. As wave number is increased to the high values, it is seen that

TS mode's (thick lines) and Yih mode's (thin lines) neutral stability curves start to coalesce at a point around $Re = 1180$ for $l = 1$. However, for $l = 0.5$ Yih mode and TS mode are quite distinct. For $l = 2$, the unstable region for TS mode disappears after $Re \cong 120$ and a stable region for large wave numbers are observed. As it is understood, the critical Reynolds number, which is indicator of stability, decreases as fluid thickness increases.

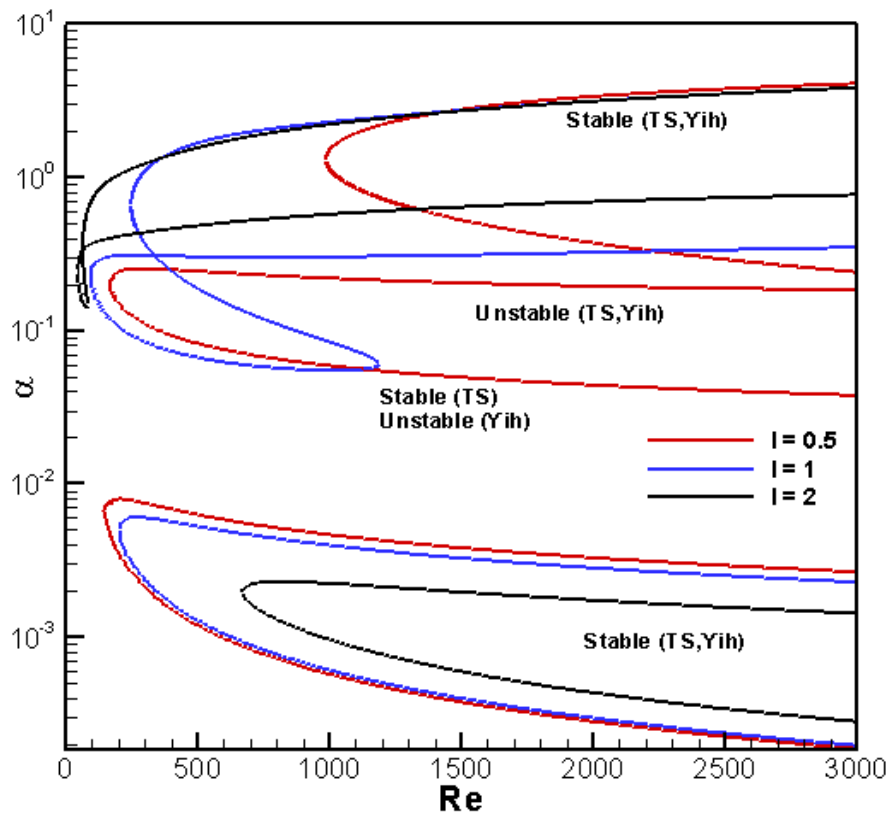


Figure 4.5 Effect of thickness ratio l ($m = 5, r = 1, S = 0, F = 0$)

In Figure 4.6, the effect of density stratification is observed. At low wave number values up to a certain value of r , in this case it is 50, effect of density ratio is not observed. After $r = 50$, the stable region decreases. For $r = 1000$, the stable region is not observed. For high values of wave number ($1 < \alpha < 10$), the stable region is immediately disappears, when r is not equal to 1. These results reveal that density has a destabilizing effect at high and low wave numbers.

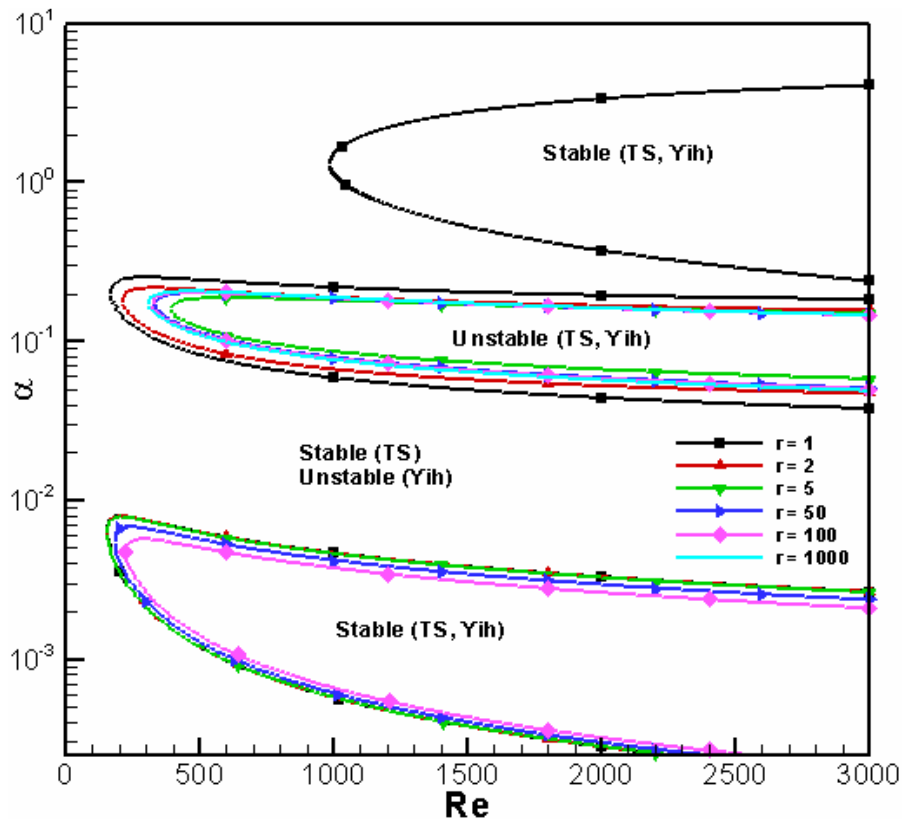


Figure 4.6 Effect of density ratio r ($m = 5, l = 0.5, S = 0, F = 0$)

From the Figure 4.7, stabilizing effect of density stratification for TS mode is observed. However, it is interesting to see that the most stable configuration is observed when $r = 5$. The values higher than 5, is less stable. Moreover, the shape of the neutral stability curve does not vary whatever the r value is. As it is seen, neutral stability curves are very similar for density ratios of 50, 100 and 1000.

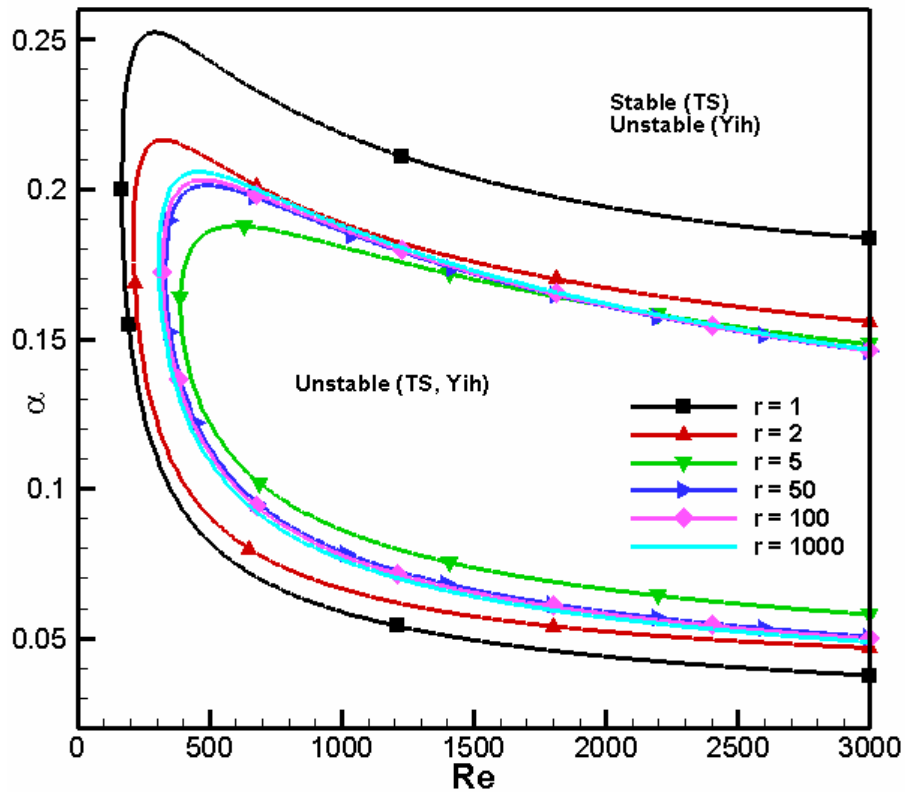


Figure 4.7 Effect of density ratio r on TS mode ($m = 5, l = 0.5, S = 0, F = 0$)

In Figure 4.8, the effect of surface tension is seen. For low wave numbers surface tension has no effect. The neutral stability curves are same for all surface tension values. For high values of wave number when $S = 0$, the familiar neutral stability curves are observed. When value of S is increased, surprisingly, cut-off curves are observed. The area under the curve is unstable, whereas upper region is unconditionally stable. In addition to this, as S value is increased the unstable domain decreases. It implies that surface tension has a strong stabilizing effect at moderate and high wave number region. Since surface tension is strongly dependent on surface curvature, it is quite normal to see the effects of surface tension on short waves. For TS mode, lower branch of neutral stability curves remain unaltered. The upper branches of the curves are same for all S values, except 1. For Reynolds numbers approximately larger than 1750, upper branch of $S = 1$ curve differs. The unstable region increases for this value. Therefore, increase in S has a destabilizing effect in the defined region.

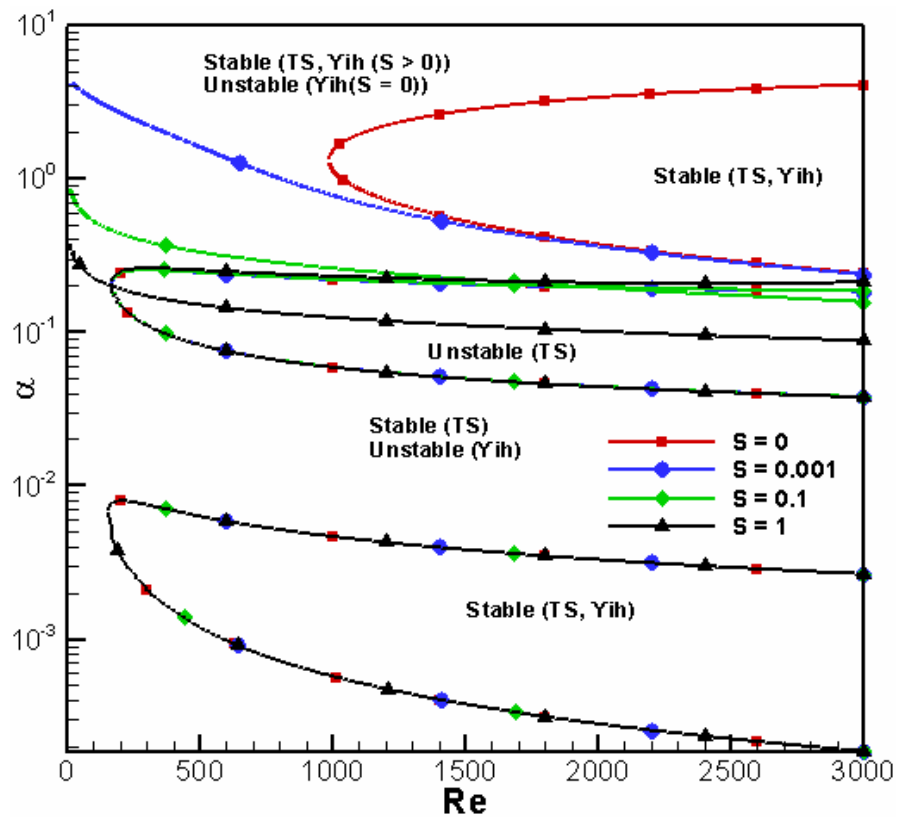


Figure 4.8 Effect of surface tension parameter S ($m = 5, l = 0.5, r = 1, F = 0$)

In Figure 4.9, the effect of gravity is observed. According to the results, the effect of gravity variation is not observed at low and high wave numbers. As F is increased further, it is seen that existence of gravity has a stabilizing effect on TS mode.

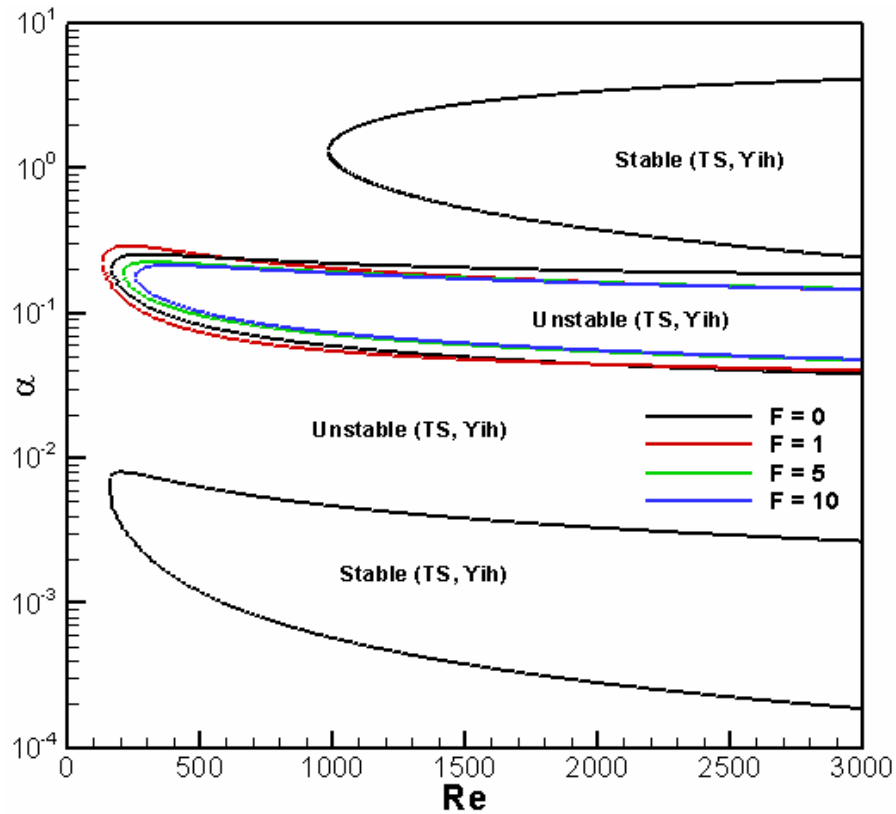


Figure 4.9 Effect of Froude number F ($m = 5, l = 0.5, S = 0, r = 1$)

Finally, the effect of non-Newtonian lower fluid is seen in Figure 4.10. For low wave numbers, stable region of Yih mode remains unaltered when n is changed. For high wave numbers, stable region vanishes for Yih mode whenever $n \neq 1$. For TS mode, increase in non-Newtonian (lower n) tendency has a stabilizing effect. Since the neutral stability curve shrinks, this result is in conflict with viscosity stratification results at first glance. However, if the Orr-Sommerfeld equation for lower fluid is examined, equation 3.31, it is seen that the lower fluid's velocity gradient at the interface has a power of $n-1$ and it is multiplied with m , $a_2^{n-1}m$. Since this velocity gradient term is very small, as n is decreased its value gets higher. Thus, multiplication of the term on the left with m yields higher values, when n is decreased. This is why a decrease in n has the same effect with an increase in viscosity ratio.

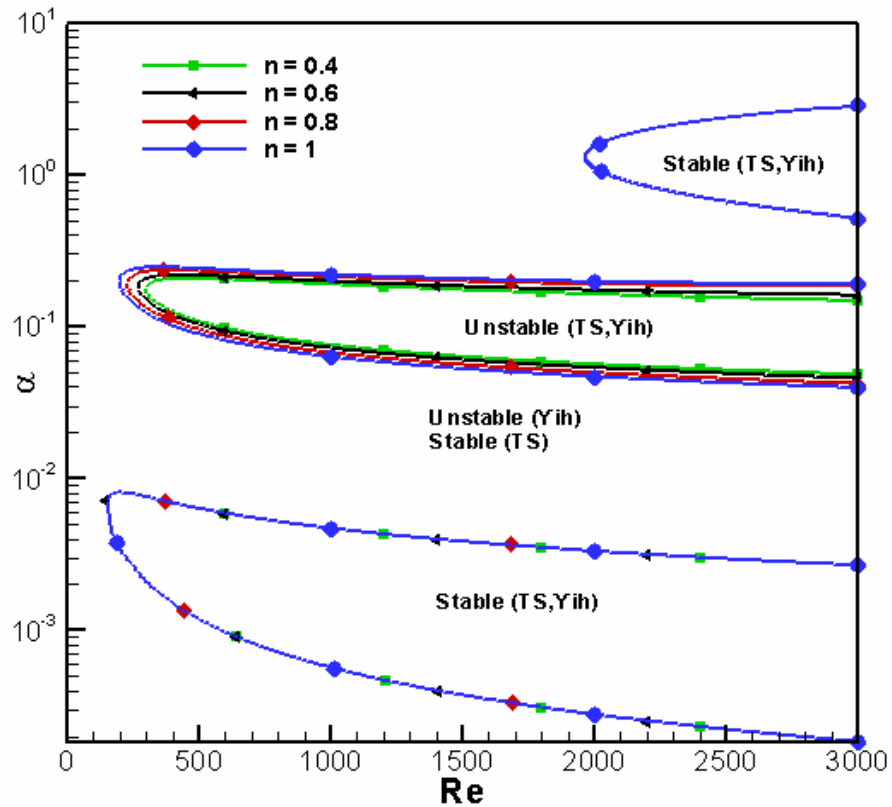


Figure 4.10 Effect of n ($m = 5, l = 0.5, S = 0, F = 0, r = 1$)

4.3 Results obtained by using turbulent boundary layer

4.3.1. Validation of the method

Miesen and Boersma [33] focused on the stability of a film which is sheared by a turbulent boundary layer and they found out the maximum temporal growth rate and corresponding wave number. In order to validate our study, a comparison is performed with their study by using the parameters that they used. The viscosity ratio, density ratio, surface tension and Froude numbers are 56.4, 824, 0.074 mN/m and 1061, respectively. Freestream velocity is 40 m/s, friction coefficient 0.02 and corresponding Reynolds number is 392. The liquid thickness 0.145 mm and channel height is 25.4 cm. Variation of amplification factor with respect to wave number as obtained in the present study is seen in Figure 4.11.

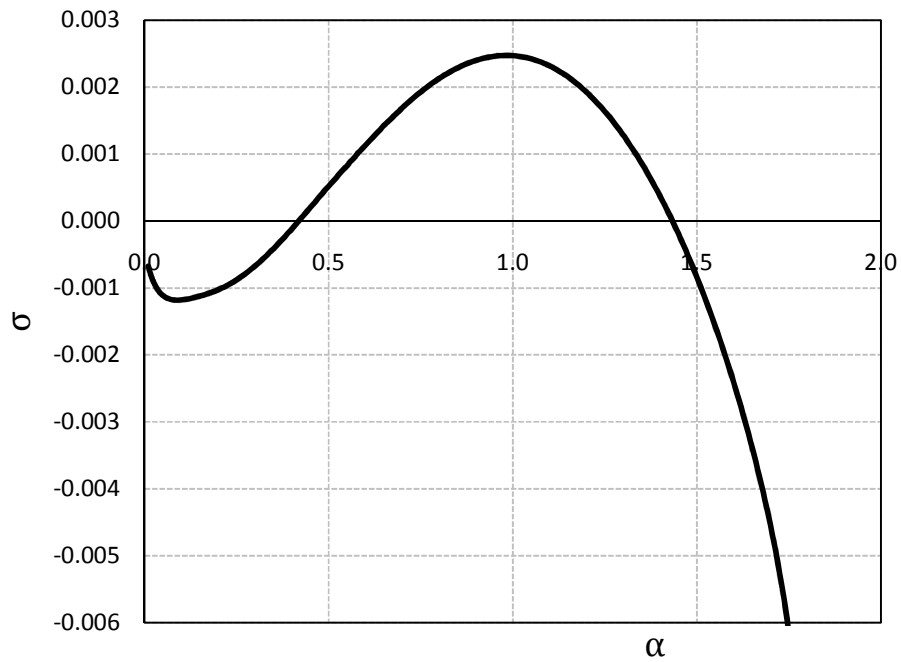


Figure 4.11 Amplification rate for Miesen and Boeresma's case for TS mode ($m = 56.4$, $r = 824$, $T^* = 0.074$ mN/m, $F = 1061$)

According to the graph $\sigma_{\max} = 2.49 * 10^{-3}$ and corresponding wave number is 0.9904. Miesen and Boersma found these values as $1.50 * 10^{-3}$ and 0.95, respectively. Their result can be seen in Figure 4.12. Since, the result that they obtained is very difficult to be read, there is an uncertainty for their result. If the results are compared, it can be said that they are in good agreement, especially for corresponding wave numbers. For maximum amplification factor, it can be concluded that they are in the same order of magnitude.

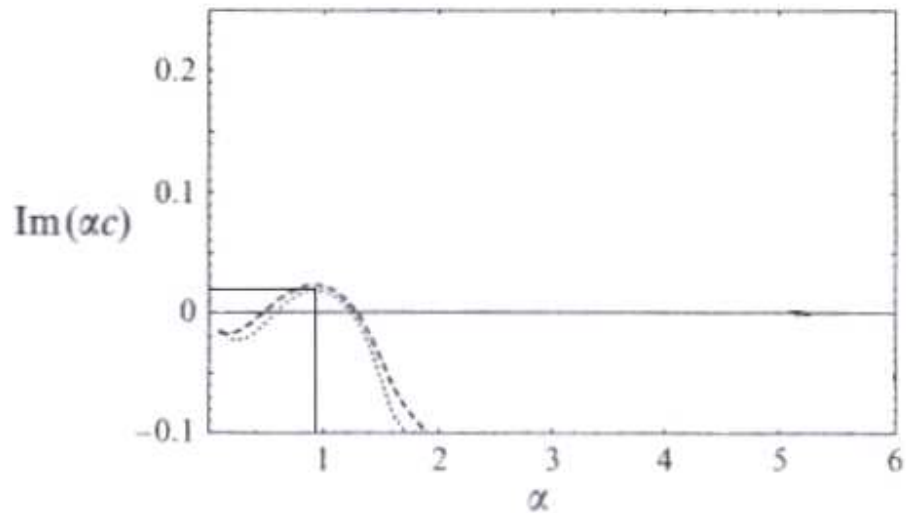


Figure 4.12 Result of Miesen and Boeresma's work for TS mode ($m = 56.4$, $r = 824$, $T^* = 0.074$ mN/m, $F = 1061$) [33]

4.3.2 Wave characteristics of de-icing and anti-icing solutions

One of main aims of this thesis is to investigate the wave characteristics of the de-icing and anti-icing solutions, to compare the results with the de/anti-icing solutions that passed aerodynamic acceptance test and to have an opinion about whether they will pass the test or not. For this, a de-icing solution (T1) and an anti-icing solution (T2), which are commercially available, were used. Sample de-icing solution (G1) and anti-icing solutions (G2) were developed. Viscosity, surface tension and density values of all solutions were measured at different temperatures (See Appendix B). Moreover, for the analysis, physical properties of air are needed. The values of parameters are tabulated in Table (4.1-4.3).

In Table 4.1, the name of the de-icing solutions, temperatures of measurements, their viscosity, surface tension and density values are given, respectively. According to the results, solution T1's viscosity is more temperature dependent. Their surface tension values are very close, but solution T1 has higher surface tension as temperature decreases. Density values do not vary too much being very close to density of water.

Table 4.1 Physical properties of the de-icing solutions that are used in the analysis at different temperatures.

Solutiom	Temperature (°C)	μ^* (cP)	T* (mN/m)	ρ^* (kg/m ³)
T1	20	24.5	40.17	1040.4
T1	0	68.8	42.09	1051.7
T1	-10	148	43.05	1056.7
G1	20	18.9	38.45	1070.2
G1	0	34.8	40.09	1083.1
G1	-10	57.1	40.86	1088.6

Table 4.2 Physical properties of the anti-icing solutions that are used in analysis at different temperatures.

Solution	Temperature (°C)	μ^* (cP)	T* (mN/m)	ρ^* (kg/m ³)
T2	20	$1138.1*\gamma^{-0.374}$	36.21	1038.2
T2	0	$1230*\gamma^{-0.295}$	37.31	1056.1
T2	-10	$1093.2*\gamma^{-0.227}$	37.86	1061.8
G2	20	$1722*\gamma^{-0.484}$	38.15	1038.2
G2	0	$5499*\gamma^{-0.608}$	39.90	1056.1
G2	-10	$8018*\gamma^{-0.643}$	40.78	1061.8

In Table 4.2, the name of the anti-icing solutions, temperatures of measurements, their viscosity, surface tension and density values are given, respectively. γ denotes the shear rate in 1/s. According to viscosity results, consistency index, k, is more dependent on temperature for G2 solution. It increases as temperature decreases. However, for T2 solution, it does not vary too much with temperature. It varies between 1000-1250 cP. Moreover, contrary to T2 solution, shear thinning tendency of G2 solution increases as temperature decreases. T2 solution has lower surface tension and densities are same because they are assumed to have same glycol and water concentration.

In Table 4.3, physical properties of air are given.

Table 4.3 Physical properties of air at different temperatures.

Fluid	Temperature (°C)	μ^* (cP)	ρ^* (kg/m ³)
Air[42]	20	0.0182	1.204
Air[42]	0	0.0171	1.292
Air[42]	-10	0.0167	1.304

The numerical code for linear stability analysis requires viscosity and density ratios, fluid layer thickness and surface tension parameter as input. For all solutions the neutral stability curves, which are in Appendix C, were obtained at given thickness and temperature values.

In Tables (4.4-4.7), the columns depict temperature, fluid thickness, critical Reynolds number, critical wind speed, that is the speed above which unstable waves will exist at the interface, wavelength and wave speed at critical Reynolds number, respectively. The wave characteristic results for Type-1 fluids are obtained and tabulated in Table 4.4 and Table 4.5.

According to the results, critical Reynolds numbers' of the fluids that have the same thickness increases as temperature decreases. However, one cannot say the exact behavior for critical wind speeds. Generally speaking, the results vary around 9 m/s and 11 m/s. Moreover, it is understood that temperature of ambient air, which is effective on the kinematic viscosity, is a crucial factor for stability analysis. Wavelengths of the interface increase as temperature decreases at the same fluid thickness. The wave speed values, which is an important parameter for flow-off properties, decreases when both temperature and fluid thickness decreases. If the results for G1 and T1 fluids are compared, unstable waves on G1 fluids are observed earlier, since they have lower critical Reynolds number. But, as the fluid thickness decreases critical Reynolds numbers become similar and this situation is fairly independent of temperature. Moreover, this comment is supported by the critical wind speed results. G1's critical wind speeds are mostly less than T1's. Wavelengths of these fluids are similar but generally T1's values are slightly higher. However, G1 fluid leaves the aircraft surface faster, approximately two times faster at

0°C and – 10°C. this is a well desired performance criterion for de/anti-icing solutions. In Table 4.6 and 4.7 wave characteristic results of T2 and G2 solutions are given.

Table 4.4 Wave characteristics of T1 solution

Temperature (°C)	d_2^* (mm)	Re_{cr}	U_{cr}^* (m/s)	λ^* (mm)	c_r^* (mm/s)
20	2.4	1537.6	9.6845	21.94	98.35
20	1.8	1138.3	9.5594	26.73	51.72
20	1.2	854.6	10.7653	27.10	24.76
0	2.4	1917.7	10.5756	26.73	40.08
0	1.8	1266.2	9.3103	40.99	12.63
0	1.2	945.4	10.4272	30.18	7.70
-10	2.4	2022.2	10.4852	29.13	17.51
-10	1.8	1307.7	9.0406	36.49	6.53
-10	1.2	981.3	10.1762	30.59	3.48

Table 4.5 Wave characteristics of G1 solution

Temperature (°C)	d_2^* (mm)	Re_{cr}	U_{cr}^* (m/s)	λ^* (mm)	c_r^* (mm/s)
20	2.4	1447.2	9.1151	21.12	110.33
20	1.8	1113.1	9.3477	24.85	64.93
20	1.2	848.6	10.6897	24.91	34.63
0	2.4	1791.3	9.8785	23.02	77.53
0	1.8	1254.4	9.2235	35.24	28.23
0	1.2	942.1	10.3908	29.28	15.69
-10	2.4	1974.5	10.2379	25.41	48.94
-10	1.8	1310.3	9.0586	34.89	17.94
-10	1.2	986.7	10.2322	29.20	9.65

Table 4.6 Wave characteristics of T2 solution

Temperature (°C)	d_2^* (mm)	Re_{cr}	U_{cr}^* (m/s)	λ^* (mm)	c_r^* (mm/s)
20	2.4	1796.2	11.3133	32.41	1.00
20	1.8	1175.3	9.8701	35.43	0.39
20	1.2	864.3	10.8875	31.63	0.22
0	2.4	1945.37	10.7281	30.03	1.18
0	1.8	1265.4	9.3044	39.71	0.40
0	1.2	940.6	10.3743	30.56	0.25
-10	2.4	2012.9	10.4370	28.94	1.66
-10	1.8	1303.6	9.0123	34.17	0.63
-10	1.2	973.5	10.0953	30.35	0.34

Table 4.7 Wave characteristics of G2 solution

Temperature (°C)	d_2^* (mm)	Re_{cr}	U_{cr}^* (m/s)	λ^* (mm)	c_r^* (mm/s)
20	2.4	1804	11.3624	27.65	0.302581
20	1.8	1178.8	9.8995	38.31	0.096025
20	1.2	867.4	10.9266	32.08	0.063265
0	2.4	1953	10.7702	29.83	0.004377
0	1.8	1267.72	9.3215	39.04	0.001210
0	1.2	944	10.4118	30.55	0.001008
-10	2.4	2022.8	10.4883	29.13	0.000662
-10	1.8	1305.18	9.0232	39.13	0.000168
-10	1.2	978.2	10.1440	30.08	0.000156

According to the above results, similar comments can be mentioned. But it is interesting to see that for all types of fluids, whatever it is Newtonian or pseudoplastic, Reynolds numbers become similar as fluid thickness decreases. This is also supported by critical wind speed results. Wavelengths of pseudoplastic solutions are fairly similar but generally

they are longer than Newtonian solutions. As an interesting result, critical wave speeds are much lower, typically two orders of magnitude lower compared to the Newtonian fluids. If the results for G2 and T2 solutions are compared, unstable waves are observed at similar wind speeds. Moreover, wavelengths are similar. The main difference between these solutions is observed at critical wave speeds. As it is mentioned above, waves at pseudoplastic solutions are slower than Newtonian solution. In this case the velocity difference between T2 and G2 fluids is quite obvious. This result claims that G2's flow-off property is so bad that it could stick to the surface of aircrafts.

During the development process of anti-icing solutions, the parameters that affect the physical properties of the solutions were well understood. If Table 4.1 is analyzed, it is seen that G2 solution's viscosity at low shear rates is obviously higher than T2's, although the fact that shear thinning tendency of G2 is higher. If the mentioned viscosity value is decreased to a certain value, the desired values in wave characteristics can be obtained. In order to do that, the following procedures can be applied:

- A) Decrease the polymer ratio in the solution,
- B) Change the pH value,
- C) Decrease the surfactant ratio in the solution.

CHAPTER 5

CONCLUSIONS AND RECOMMENDATIONS

5.1 General conclusions

This thesis was devoted to topics in two disciplines. Firstly, the development process of de-icing and anti-icing solution, which is related to Chemical Engineering, was investigated. In this part, chemical additives that are widely used in industry were examined in order to obtain the desired solutions. Experiments were based on measurements of viscosity, surface tension and freezing point of sample solutions. Secondly, the behavior of de-icing and anti-icing solutions on wing surface was simulated. The mathematical model and solution method that is related to Aerospace Engineering were summarized. After a parametric study that investigates the effect of physical properties on the stability of two-layer flows and comparison of wave characteristics of developed and commercially available de-icing and anti-icing solutions were performed.

In solution development process, firstly, variations of physical properties were observed at different glycol and water concentrations. Then, functional chemicals (S, C, pH) were added to the mixtures. Since, the main aim was to see their effects, exact amount of functional chemicals in solution was not a concern. After that, physical properties of the solutions were measured when functional chemicals were used together. In this part, amount of functional chemicals in the solution was another important issue. Many experiments were performed in order to obtain the final composition.

Since the only difference between de-icing and anti-icing solutions is the addition of polymer in terms of chemical composition, studies for anti-icing solutions started with polymer concentration effect. Although viscosity results were better than expected, pH value of the solutions was low. In order to have solutions that are in neutral pH region and measurable viscosity, polymer concentration was decreased and a basic chemical, NaOH, was used in order to have desired pH value. After that, solution was prepared at different

glycol and water concentration in order to see the viscosity behavior. Finally, effect of surfactant on surface tension and viscosity was investigated. A final composition for anti-icing solution was not declared, since it is not completely ready. It is important to mention that, in this thesis the summary of the best results of the development process were discussed. If further information is needed, the reader must refer to Barış Erdoğan's M. S. [19].

The second part of the study started with the mathematical modeling and the solution method for linear stability analysis of two-layer flows. Mathematical modeling was based on derivations of Orr-Sommerfeld equation for power-law fluids. In this study, the mentioned equation was found and compared with the one in literature [40]. The solution method was summarized. Then, the available Fortran code was modified by changing the function minimization subroutine.

The numerical results consist of two parts. In the first part, a parametric study was performed in order to see effect of physical properties on stability. The results were obtained by changing a physical property while keeping the others constant. Whenever there is a viscosity difference between the two fluids Yih modes are of mathematical interest since for large values of m it disappears. As interface is moved away from the wall, TS mode disappears and stable region of Yih mode shrinks to left. TS mode is more stable as density ratio is increased. But, this increase has destabilizing effect on Yih mode. Since surface tension is dependent on surface curvature, it is quite normal to see effect of it on large wave numbers. When $S \neq 0$, two regions, one is stable the other is unstable, are observed. As S value is increased, unstable region reduces in size. At the existence of gravity, Yih modes disappear while the same parameter has a stabilizing effect for TS mode. Finally, increase in shear thinning tendency of the lower fluid causes more stable flow. At first glance, it conflicts with viscosity stratification results. However, the mathematical reasoning explains the phenomena well.

In the second part, wave characteristics of developed and commercially available de-icing and anti-icing solutions were compared. Since the code requires viscosity, density, surface tension values of solutions, these values were obtained at different temperatures. According to the results, viscosity of developed de-icing fluid is more temperature dependent. Both developed and commercially available solutions have similar surface tension and density values. For anti-icing solutions, developed one has a viscosity that is

more temperature dependent. But, commercially available solution has a viscosity that varies between 1000 cP and 1200 cP. However, shear thinning tendency of developed solution increases as temperature decreases. For commercially available solution, this situation is vice versa. Similar to de-icing solutions, they have close surface tension and density values.

Developed de-icing solution flows-off earlier and faster than commercially available one according to the critical Reynolds number and critical wave speed results. Since the developed one has lower viscosity at all temperatures, this result is expected. Developed anti-icing solution has similar critical Reynolds number values to commercially available one even at low temperatures. This similarity at low temperatures can be explained with the increase in shear thinning tendency of the developed anti-icing although it has higher viscosity at low shear rates. However, critical wind speed results of developed de-icing solutions reveal that, this solution cannot flow-off as easy as commercially available one does.

5.2 Recommendations for better solutions

In order to have more efficient solutions, chemical composition and physical properties of de-icing and anti-icing solutions can be changed.

Desired de-icing and anti-icing solutions can be prepared in infinitely many combinations of chemical additives. But, the main aim is to find the optimum composition for desired properties. If the final composition of de-icing solution is concerned, it is prepared with a glycol ratio of 90% in order to have desired viscosity range. But, addition of a polymer that increases viscosity but not the Newtonian behavior of the solution, will result in a decrease in glycol concentration. If it is done, the solution's lowest operational temperature decreases and protection time increases.

According to the numerical results, developed anti-icing solution, G2, flows-off wing surface very slowly at low temperatures compared to commercially available anti-icing solution, T2, as G2 solution's viscosity at low shear rates is approximately 7 times higher than that of T2. In order to overcome this, temperature dependency of G2 solution should be carefully investigated. In order to decrease viscosity of this solution, a few minor changes can be done. These are:

- A) Decrease the polymer ratio in the solution,
- B) Change the pH value,
- C) Decrease the surfactant ratio in the solution.

If the polymer ratio in the solution is decreased, both the viscosity at low shear rates and shear thinning tendency, which is an important property for better flow-off property, decrease. Therefore, the double effect of the polymer concentration should be carefully examined. As discussed in Chapter 2, pH value of the solution is a dominant factor on viscosity. Therefore, it can be changed in order to decrease viscosity. But it should be remembered that, pH value should be in basic range, so that its corrosive effect shall be minimum. Finally, surfactant ratio can be decreased for desired viscosity. But, it is a limited solution to viscosity problem, since surfactant is used for surface tension reduction.

5.3 Recommendations for future work

With the help of this study, a strong background has been constructed for production of de-icing and anti-icing solutions. In order to be able to produce these solutions, a detailed economical analysis should be performed. Since this analysis depends on optimum chemical composition of the solutions, development process and simulation of behavior of the solutions on wings should be performed at the same time. Although mathematical modeling and solution method have been validated by using the results in literature, an experimental study will be very beneficial for wave characteristic of the solutions. Since, two-layer flows are widely used in the industry, the results of the experimental work can be very beneficial for the improvements in this area.

REFERENCES

- [1] R. Hornig, "Development of an International Standard for Safe Winter Operation", J. Aircraft, 30, pp. 14-18, January-February 1993.
- [2] Association of European Airlines, "Training Recommendations and Background Information for De-Icing/Anti-Icing of Aircraft on Ground", 3rd Edition, September 2006.
- [3] E. G. Hill and T. A. Zierden, Aerodynamic Effects of Aircraft Ground De/Anti-Icing Fluids, J. Aircraft, 30, pp. 24-34, January-February 1993.
- [4] J. F. Ross and J.T. Connolly, "Contrasting Requirements for Type-II De/Anti-Icing Fluids", J. Aircraft, 30, pp. 10-13, January-February 1993.
- [5] J. J. Reinmann, "Aerodynamic Effects of Deicing and Anti-Icing Fluids", J.Aircraft, 30, pp. 8-9, January-February 1993.
- [6] S. Özgen, M. Carbonaro and G. S. R. Sarma, "Experimental Study of Wave Characteristics on a Thin Layer of De/Anti-Icing Fluid, Phys. Fluids", 14, pp. 3391-3402, October 2002.
- [7] A. Beisswenger and J. L. Laforte, "Endurance and Aerodynamic Performance Certification of Aircraft De/Anti-icing Fluids", SAE International, 2003.
- [8] Dow, "UCAR Ultra Type-IV Fluid", Form No. 183-00003-1004AMS, October 2004.
- [9] Dow. "UCAR Concentrate "55/45" Type-I Fluid", Form No. 183-00024-0704AMS, July 2004.
- [11] Guidelines for Aircraft Ground Icing Operations, 2nd Edition, April 2005.
- [12] Patent no. 4358389, "Agent for De-Icing and Protecting Against Icing-Up", October 1982.
- [13] Patent no. 4744913, "De-Icing and Anti-Icing Fluid for Aircraft", May 1988.

- [14] Patent no. 5118435, "Anti-Icing Compositions Containing Thickener Blend Having Polyacrylic Acid and Copolymer Of Acrylic Acid and Hydrophobic Vinyl Monomer" February 1992.
- [15] Patent no. 5389276, "Aircraft Deicing Fluid with Thermal and Ph-Stable Wetting Agent", February 1995.
- [16] Patent no. 5435930, "Deicer/Anti-Icer Compositions for Aircraft", July 1995.
- [17] Patent no. 7037442, "De-icing Composition and Anti-icing Composition, Thickened with Sheet Silicates" May 2006.
- [18] J. J. Johnson, N. Varney and M. S. Switzenbaum, "Comparative Toxicity of Formulated Glycol Deicers and Pure Ethylene and Propylene Glycol", August 2001.
- [19] B. Erdoğan, "Production and Development of De/Anti-Icing fluids for Aircraft", M. S. dissertation, METU, September 2008
- [20] O. Reynolds, "An Experimental Investigation of The Circumstances Which Determine Whether The Motion of Water Shall Be Direct or Sinuous, and of The Law of Resistance in Parallel Channels", Philosophical Transactions of the Royal Society of London, 174, pp. 935-982, 1883
- [21] W. M.F. Orr, "The Stability or Instability of The Steady Motions of A Perfect Liquid and of A Viscous Liquid", Proc. R. Ir. Acad. Sect. B, Bio. Geo. Chem., pp. 9-138, 1907.
- [22] A. Sommerfeld, "Ein Beitrag zur Erklärung der turbulenten Flüssigkeitsbewegungen", Atti del 4.Congr. Internat.dei Mat. III, Roma, pp 116-124, 1908.
- [23] G. B. Schubauer and H. K. Skramstad, "Laminar Boundary-Layer Oscillations and Transition on a Flat Plate", J. Res. Natl. Bur. Stand., 38, pp. 251-292, 1947.
- [24] P. G. Drazin, "Introduction to Hydrodynamic stability", Cambridge University Press, 2002.
- [25] L. S. Cohen and T. J. Hanratty, "Generation of Waves in The Concurrent Flow of Air and A Liquid", J. AIChE, 11, pp. 138-144., January 1965.

- [26] C. S. Yih, "Instability Due to Viscosity Stratification", *J. Fluid Mech.* 27, pp. 337-352, 1967.
- [27] P. J. Blennerhassett, "On The Generation of Waves by Wind", *Phil. Trans. R. Soc. Lond., A* 298, pp. 451-494, December 1980.
- [28] A. P. Hooper and W. G. C. Boyd, "Shear-Flow Instability at The Interface Between Two Viscous fluids, *J. Fluid Mech.*, 128, pp. 507-528, 1983.
- [29] T. J. Hanratty, "Interfacial Instabilities Caused by Air Flow", Academic Press, New York, pp. 221-259, 1983.
- [30] S.G. Yiantsios and B.G. Higgins, "Linear Stability of Plane Poiseuille Flow of Two Superposed Fluids", *Phys. Fluids*, 31, pp. 3225-3238, November 1988.
- [31] H. Ludwig and H. Hornung, "The Instability of A Liquid Film on A Wall Exposed to An Air Flow", *J. Fluid Mech.*, 200, pp. 217-233, 1989.
- [32] C. S. Yih, "Wave Formation on A Liquid Layer for De-Icing Airplane Wings", *J. Fluid Mech.*, 212, pp. 41-53, 1990.
- [33] R. Miesen and B. J. Boersma, "Hydrodynamic Stability of A Sheared Liquid Film", *J. Fluid Mech.*, 301, pp. 175-202, 1995.
- [34] S. N. Timoshin, "Instabilities in A High-Reynolds Number Boundary Layer on A Film-Coated Surface", *J. Fluid Mech.*, 353, pp. 163-195, 1997.
- [35] N. A. Pelekasis and J. A. Tsamopoulos, "Linear Stability of A Gas Boundary Layer Flowing Past A Thin Liquid Film That Grows over A Flat Plate", *J. Fluid Mech.*, 436, pp. 321-352, 2001.
- [36] S. Özgen, G. Degrez and G. S. R. Sarma, "Two-Fluid Boundary Layer Theory", *Phys. Fluids*, 10, pp. 2746-2757, November 1998.
- [37] S. Özgen, M. Carbonaro and G. S. R. Sarma, "Experimental Study of Wave Characteristics on a Thin Layer of De/Anti-Icing Fluid", *Phys. Fluids*, 14, pp. 3391-3402, October 2002.

- [38] K. C. Sahu, P. Valluri, P. D. M. Spelt and O. K. Matar, "Linear Instability of Pressure-Driven Channel Flow of A Newtonian and A Herschel-Bulkley Fluid", *Phys. Fluids* 19, pp. 122101/1-11, 2007.
- [39] S. Özgen, "Coalescence of Tollmien-Schlichting and Interfacial Modes of Instability in Two-Fluid Flows", *Phys. Fluids*, 20, pp. 044108/1-13, 2008.
- [40] S. Özgen, "Two-Layer Flow Stability in Newtonian and Non-Newtonian Fluids", Ph. D. Dissertation, Univeriste Libre de Bruxelles, Von Karman Institute for Fluid Dynamics, 1999.
- [41] G. S. Hendrickson and E. G. Hill, "Effect of De/Anti-Icing Fluids on Airfoil Characteristics", Technical report, Boeing Report, 1987.
- [42] B. R. Munson, D. F. Young and T. H. Okiishi, "Fundamentals of Fluid Mechanics", 4th edition, John Wiley and Sons, 2002.
- [43] Kilfrost DF Plus 88, "Material Safety Data Sheet", April 2005.
- [44] Kilfrost ABC-3, "Material Safety Data Sheet", March 2000.

APPENDIX A

DERIVATION OF INTERFACE CONDITIONS FOR TWO-LAYER FLOW

Continuity of normal velocity:

Normal disturbance velocity, \hat{v} , is continuous at the interface.

$$\hat{v}_1(0) = \hat{v}_2(0), \quad (\text{A. 1})$$

$$\overline{\varphi}(0) = \overline{\chi}(0). \quad (\text{A. 2})$$

Continuity of the streamwise velocity:

Since U' is discontinuous at the interface, the equation should be satisfied at the disturbed interface at $y = \xi$.

$$u_1(\xi) = u_2(\xi), \quad (\text{A. 3})$$

$$U_1(\xi) + \hat{u}_1(\xi) = U_2(\xi) + \hat{u}_2(\xi). \quad (\text{A. 4})$$

Velocities can be expanded in Taylor series around $y = 0$, as follow:

$$u_1(\xi) = U_1(0) + \hat{u}_1(0) + U_1' \xi + \dots \dots \dots, \quad (\text{A. 5})$$

$$u_2(\xi) = U_2(0) + \hat{u}_2(0) + U_2' \xi + \dots \dots \dots. \quad (\text{A. 6})$$

If normal velocity and ξ are defined as follows:

$$\hat{v} = \frac{\delta \xi}{\delta t} + U_0 \frac{\delta \xi}{\delta x}, \quad (\text{A. 7})$$

$$\xi(x, t) = \xi_0 e^{i\alpha(x-ct)}, \quad (\text{A. 8})$$

and A.8 is integrated into A.7, the following equation is obtained:

$$-i\alpha\varphi(0)e^{i\alpha(x-ct)} = -i\alpha c\xi_0 e^{i\alpha(x-ct)} + U_0 i\alpha\xi_0 e^{i\alpha(x-ct)}. \quad (\text{A. 9})$$

This yields the equation below:

$$\xi(x, t) = \frac{\varphi(0)}{c - U_0} e^{i\alpha(x-ct)} = \frac{\chi(0)}{c - U_0} e^{i\alpha(x-ct)} \quad (\text{A. 10})$$

If equation A.10 is added to the A.5 and A.6, then arrangement is made, the equation below is obtained:

$$\varphi'(0) - \chi'(0) = (a_2 - a_1) \frac{\varphi(0)}{c - U_0}. \quad (\text{A. 11})$$

Continuity of shear stress:

Shear stress at the interface is equated by using formulas:

$$\tau_{xy,1}^* = -k_1^* \left[2 \left[\left(\frac{\delta u_1^*}{\delta x^*} \right)^2 + \left(\frac{\delta v_1^*}{\delta y^*} \right)^2 \right] + \left[\frac{\delta u_1^*}{\delta y^*} + \frac{\delta v_1^*}{\delta x^*} \right]^2 \right]^{\frac{n_1-1}{2}} \left[\frac{\delta u_1^*}{\delta y^*} + \frac{\delta v_1^*}{\delta x^*} \right], \quad (\text{A. 12})$$

$$\tau_{xy,2}^* = -k_2^* \left[2 \left[\left(\frac{\delta u_2^*}{\delta x^*} \right)^2 + \left(\frac{\delta v_2^*}{\delta y^*} \right)^2 \right] + \left[\frac{\delta u_2^*}{\delta y^*} + \frac{\delta v_2^*}{\delta x^*} \right]^2 \right]^{\frac{n_2-1}{2}} \left[\frac{\delta u_2^*}{\delta y^*} + \frac{\delta v_2^*}{\delta x^*} \right], \quad (\text{A. 13})$$

After decomposition the flow into mean and fluctuating terms, binomial distribution and eliminating the quadratic terms are applied, the followings are obtained:

$$\tau_{xy1}^* = k_1^* \left[\frac{\delta U_1^*}{\delta y^*} + \frac{\delta \hat{u}_1^*}{\delta y^*} + \frac{\delta \hat{v}_1^*}{\delta x^*} \right]^{n_1} \quad (\text{A. 14})$$

$$\tau_{xy2}^* = k_2^* \left[\frac{\delta U_2^*}{\delta y^*} + \frac{\delta \hat{u}_2^*}{\delta y^*} + \frac{\delta \hat{v}_2^*}{\delta x^*} \right]^{n_2} \quad (\text{A. 15})$$

If binomial distribution is applied one more time, below formula is obtained:

$$k_1^* n_1 \left| \frac{dU_1^*}{dy^*} \right|^{n_1-1} \left(\frac{\delta \hat{u}_1^*}{\delta y^*} + \frac{\delta \hat{v}_1^*}{\delta y^*} \right) = k_2^* n_2 \left| \frac{dU_2^*}{dy^*} \right|^{n_2-1} \left(\frac{\delta \hat{u}_2^*}{\delta y^*} + \frac{\delta \hat{v}_2^*}{\delta y^*} \right). \quad (\text{A. 16})$$

The above equation is non-dimensionalized by using the parameters below:

$$x = \frac{x^*}{d^*}, y = \frac{y^*}{d^*}, \hat{u} = \frac{\hat{u}^*}{U_e^*}, U = \frac{U^*}{U_e^*}, \hat{v} = \frac{\hat{v}^*}{U_e^*}. \quad (\text{A. 17})$$

Finally, the desired equation is obtained:

$$\alpha^2 \phi(0) + \phi''(0) = m \frac{\alpha_2^{n_2-1} n_2}{\alpha_1^{n_1-1} n_1} [\chi''(0) + \alpha^2 \chi(0)] \quad (\text{A. 18})$$

In above equation m is defined as follows:

$$m = (k_2^*/k_1^*)(U_e^*/d^*)^{n_2-n_1}. \quad (\text{A. 19})$$

Continuity of normal stress:

Contrary to the shear stress, the difference between normal stresses at the interface should be equated by the surface tension force. The normal forces are defined as follows:

$$\sigma_{yy1}^* = -k_1^* \left[2 \left[\left(\frac{\delta u_1^*}{\delta x^*} \right)^2 + \left(\frac{\delta v_1^*}{\delta y^*} \right)^2 \right] + \left[\frac{\delta u_1^*}{\delta y^*} + \frac{\delta v_1^*}{\delta x^*} \right]^2 \right]^{\frac{n_1-1}{2}} \left[2 \frac{\delta v_1^*}{\delta y^*} \right] \quad (\text{A. 20})$$

$$\sigma_{yy2}^* = -k_2^* \left[2 \left[\left(\frac{\delta u_2^*}{\delta x^*} \right)^2 + \left(\frac{\delta v_2^*}{\delta y^*} \right)^2 \right] + \left[\frac{\delta u_2^*}{\delta y^*} + \frac{\delta v_2^*}{\delta x^*} \right]^2 \right]^{\frac{n_2-1}{2}} \left[2 \frac{\delta v_2^*}{\delta y^*} \right] \quad (\text{A. 21})$$

After decomposition the flow into mean and fluctuating terms, binomial distribution and eliminating the quadratic terms are applied, the followings are obtained:

$$\sigma_{yy1}^* = -2k_1^* \left| \frac{dU_1^*}{dy^*} \right|^{n_1-1} \frac{\delta v_1^*}{\delta y^*}, \quad (\text{A. 22})$$

$$\sigma_{yy2}^* = -2k_2^* \left| \frac{dU_2^*}{dy^*} \right|^{n_2-1} \frac{\delta v_2^*}{\delta y^*}. \quad (\text{A. 23})$$

If the parameters are added to the normal stress equation, the below formula is obtained:

$$-P_1^* - \hat{p}_1^* + 2k_1^* \left| \frac{dU_1^*}{dy^*} \right|^{n_1-1} \frac{\delta v_1^*}{\delta y^*} + P_2^* - \hat{p}_2^* - 2k_2^* \left| \frac{dU_2^*}{dy^*} \right|^{n_2-1} \frac{\delta v_2^*}{\delta y^*} = -T \frac{\delta^2 y^*}{\delta y^{*2}} \quad (\text{A. 24})$$

If non-dimensionalization is applied and (A.10) and below formulas are added to above equation:

$$\frac{\partial P}{\partial \xi} + F^{-2} = 0 \quad (\text{A. 25})$$

the following formula is obtained:

$$\begin{aligned} & i\alpha R((c - U_0)\varphi'(0) + a_1\varphi(0)) - (\varphi'''(0) - 3\alpha^2\varphi') + i\alpha Rr((c - U_0)\chi'(0) + a_2\chi(0)) \\ & + m\alpha_2^{n-1}[n\chi'''(0) - (4 - n)\alpha^2\chi'(0)] = i\alpha R[(r - 1)F^{-2} + \alpha^2 S] \varphi / (c - U_0). \end{aligned} \quad (\text{A. 26})$$

APPENDIX B

DENSITY AND SURFACE TENSION MEASUREMENTS

In order to obtain the neutral stability curves of the solutions at different temperatures, density and surface tension values at these temperatures are needed. For density ratios, Ethylene glycol product guide is used. In this guide, the freezing points of the glycol water mixture at different weight ratios are given. For T1 fluid, the weight ratio of glycol/water mixture is defined as 63/37. Moreover its density at 20 °C is given as 1041 kg/m³ [43]. By using the data in the guide, the density at 20 °C is found as 1040.4 kg/m³. However, for T2 fluid there is no exact value of glycol/water ratio. But the freezing point values of T2 fluid (pure solution and 50% mixture of the solution with water) reveal that the weight ratio of glycol/water mixture is approximately 50/50. The density of the mixture is defined as 1038 kg/m³ [42]. By using the same procedure, the density of T2 fluid is found as 1038.2 kg/m³. As it is seen the density values that are found match perfectly with producer's values. G1 and G2 solutions are prepared at a glycol /water ratio of 90/10 and 50/50 by weight, respectively. The variations of density of all solutions with temperature are given in Figures (B.1- B.3).

The surface tension measurements are performed at different and random temperatures. In order to obtain surface tension at lower temperatures, the parameter was measured immediately after samples were taken from the deep freezer. The temperatures of the solutions were measured immediately after the test was finished. If the results are analyzed, T2 solution's surface tension is 37 mN/m at 20 °C , whereas in our calculation it is found to be 36.21 mN/m [44]. However there is no result in the literature related with T1 solution's surface tension parameter. Variation of surface tension with temperature is given in Figures (B.4-B.7).

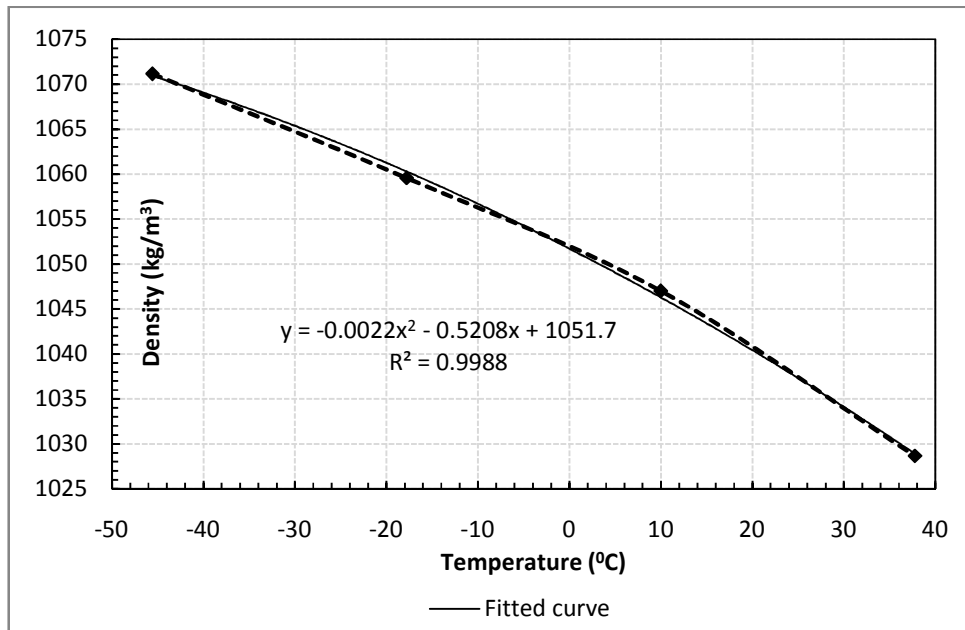


Figure B.1 Variation of density with temperature for T1 fluid

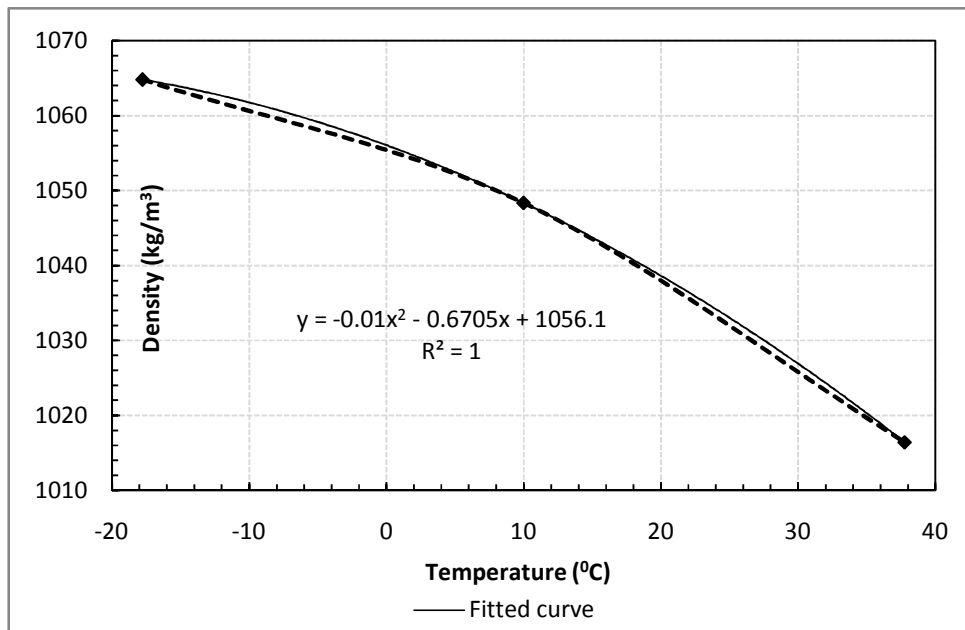


Figure B.2 Variation of density with temperature for T2 and G2 fluids

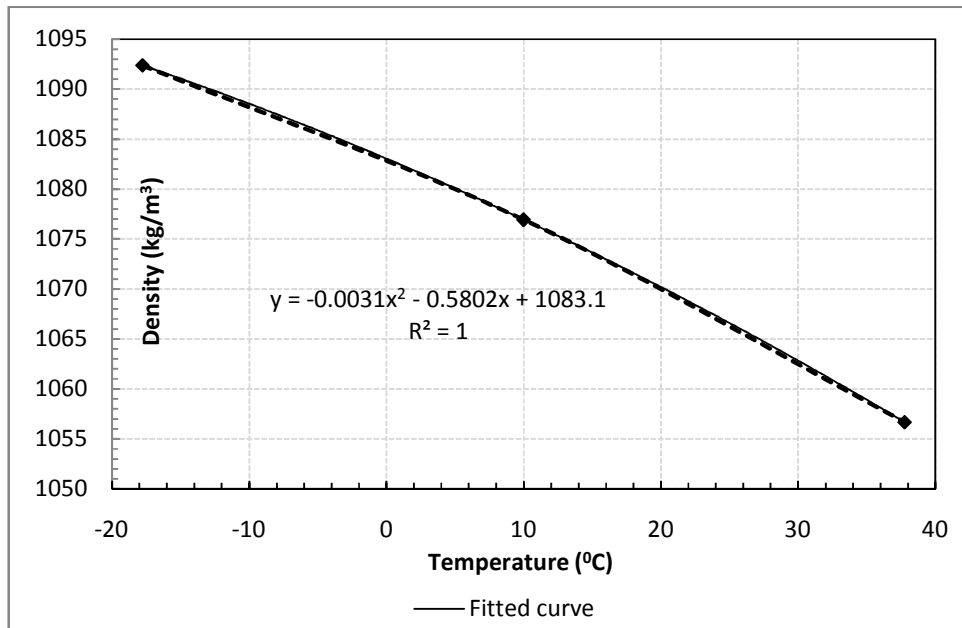


Figure B.3 Variation of density with temperature for G1 fluid

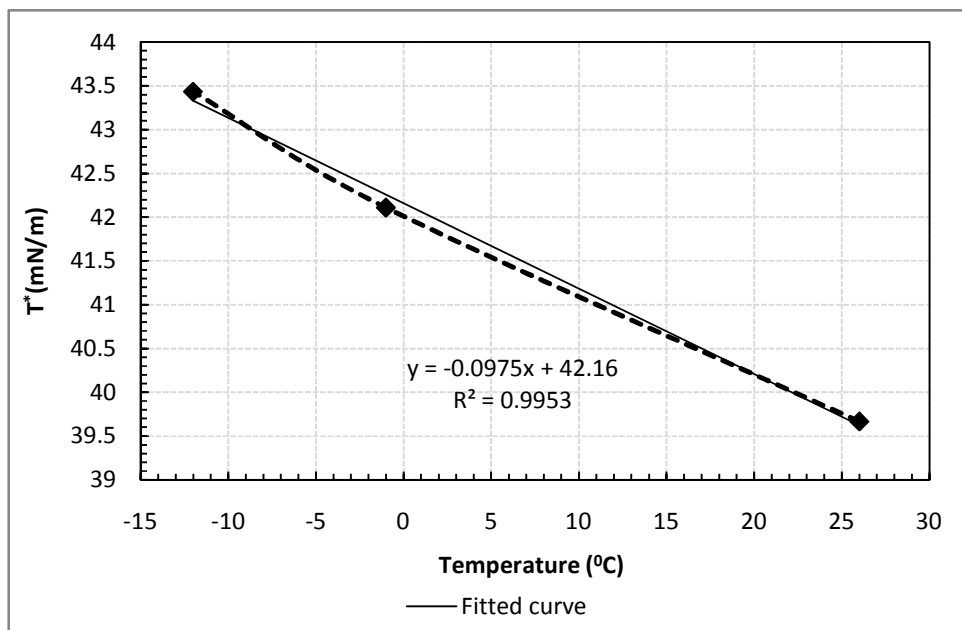


Figure B.4 Variation of surface tension with temperature for T1 fluid

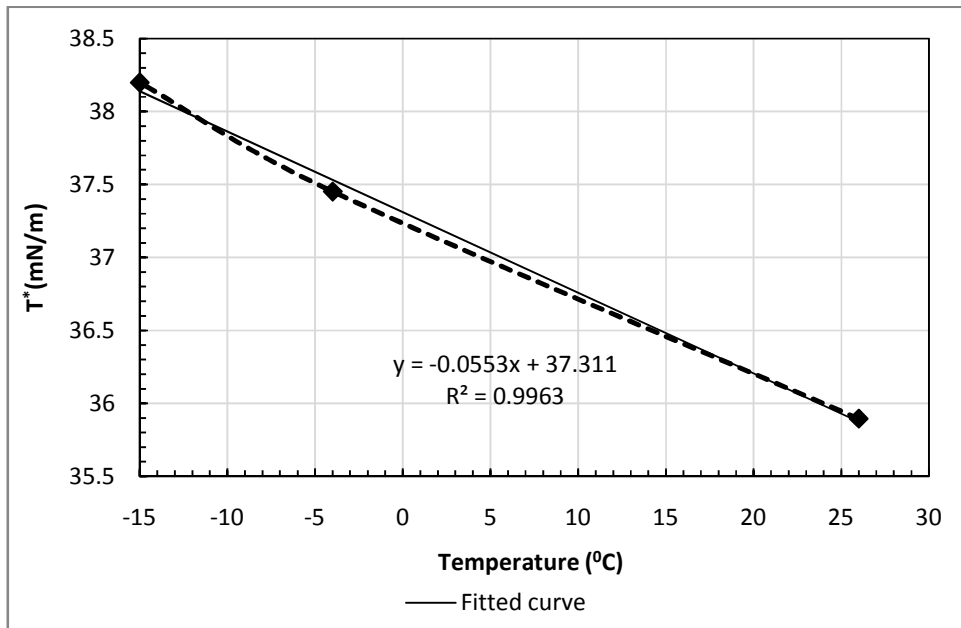


Figure B.5 Variation of surface tension with temperature for T2 fluid

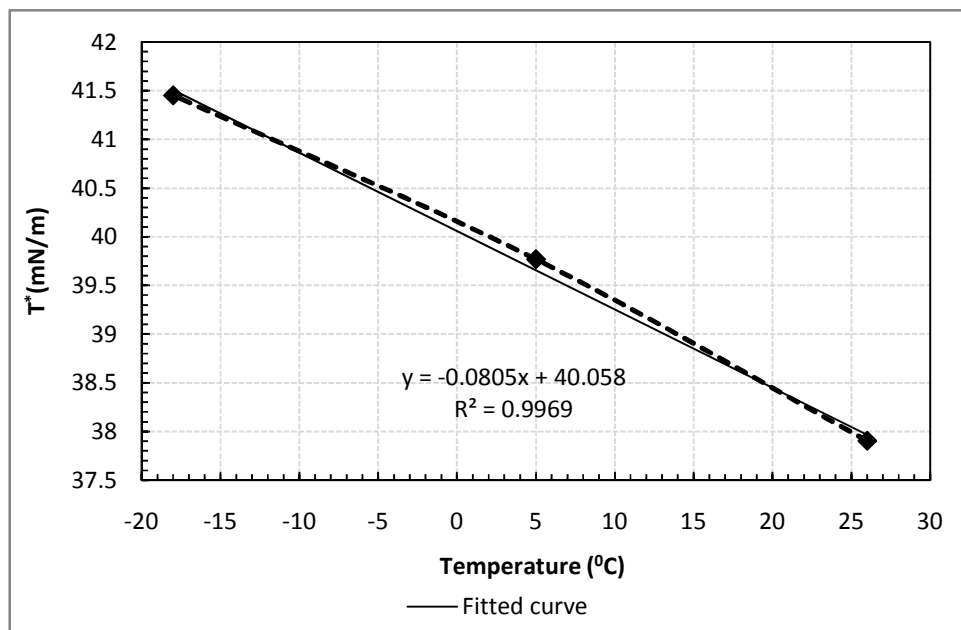


Figure B.6 Variation of surface tension with temperature for G1 fluid

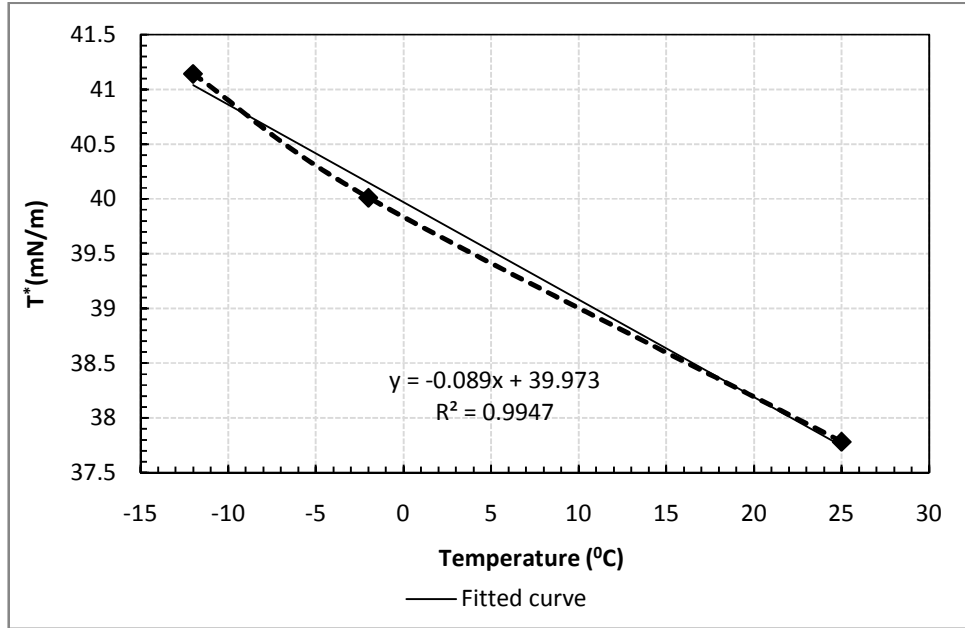


Figure B.7 Variation of surface tension with temperature for G2 fluid

APPENDIX C

NEUTRAL STABILITY CURVES FOR SAMPLE FLUIDS AT DIFFERENT THICKNESSES AND TEMPERATURES

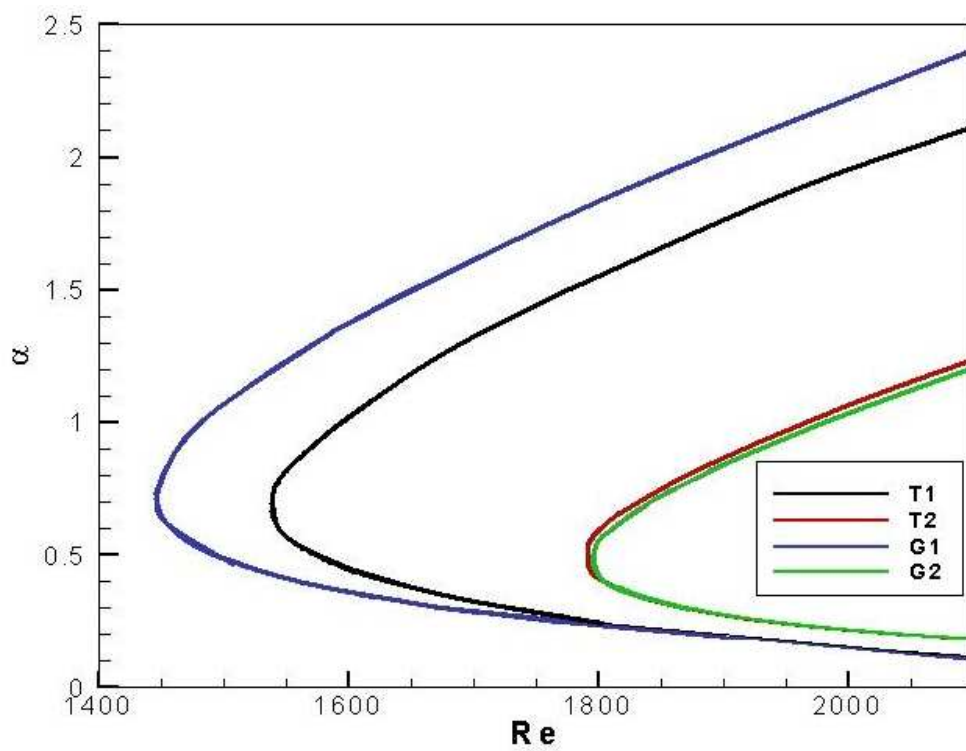


Figure C.1 Neutral stability curves for $d_2^* = 2.4$ mm. at 20°C for sample fluids

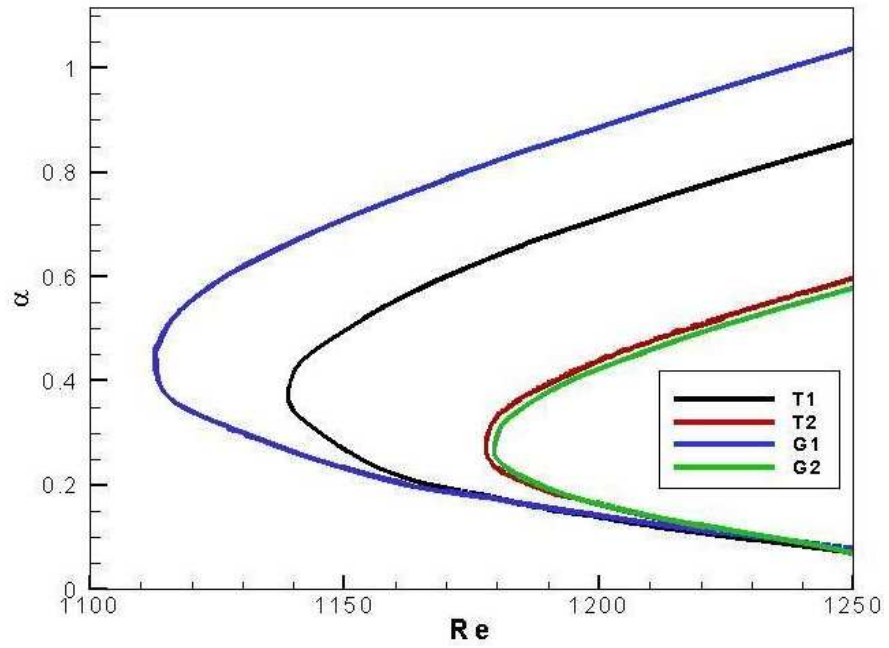


Figure C.2 Neutral stability curves for $d_2^* = 1.8$ mm. at 20°C for sample fluids

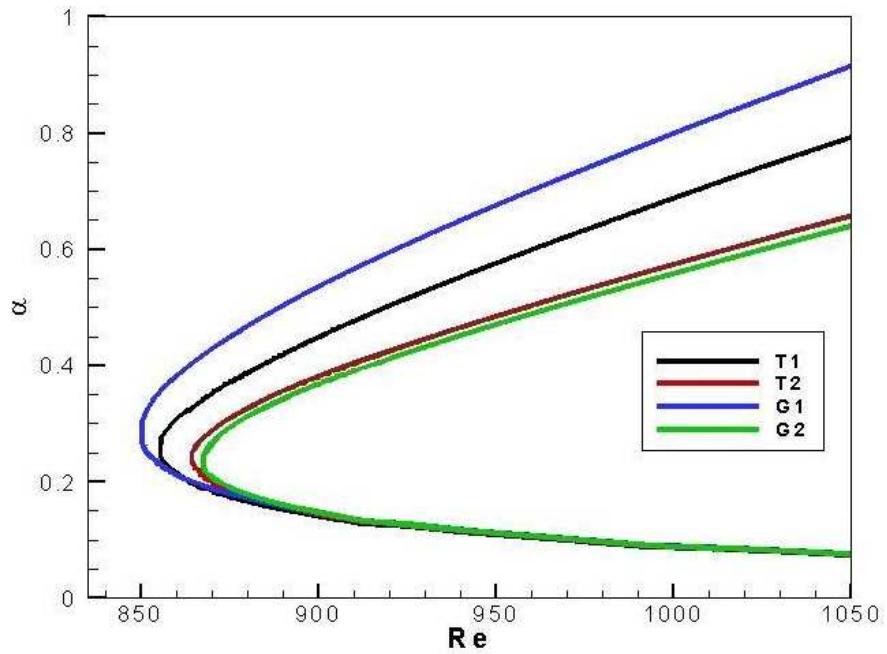


Figure C.3 Neutral stability curves for $d_2^* = 1.2$ mm. at 20°C for sample fluids

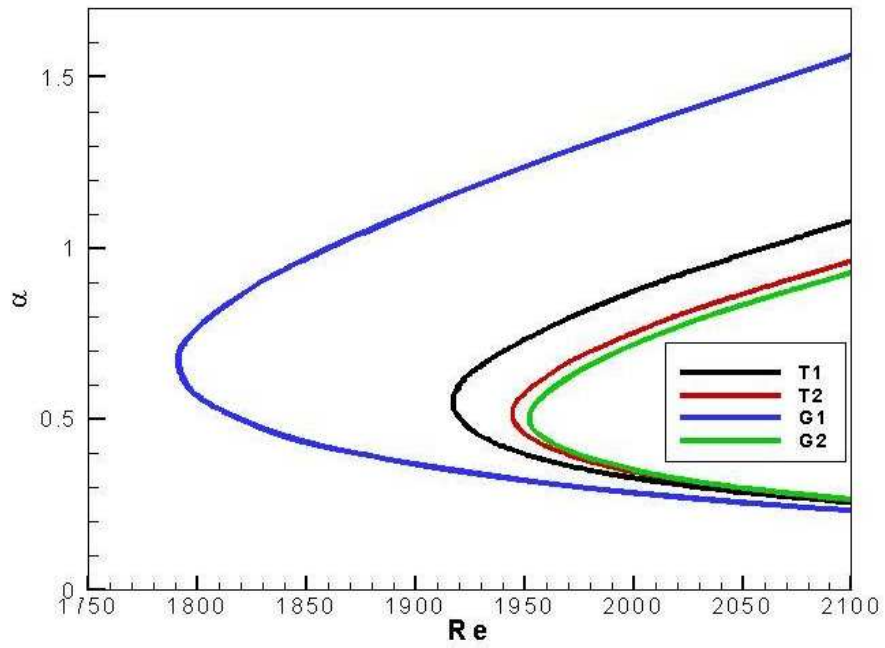


Figure C.4 Neutral stability curves for $d_2^* = 2.4$ mm. at 0°C for sample fluids

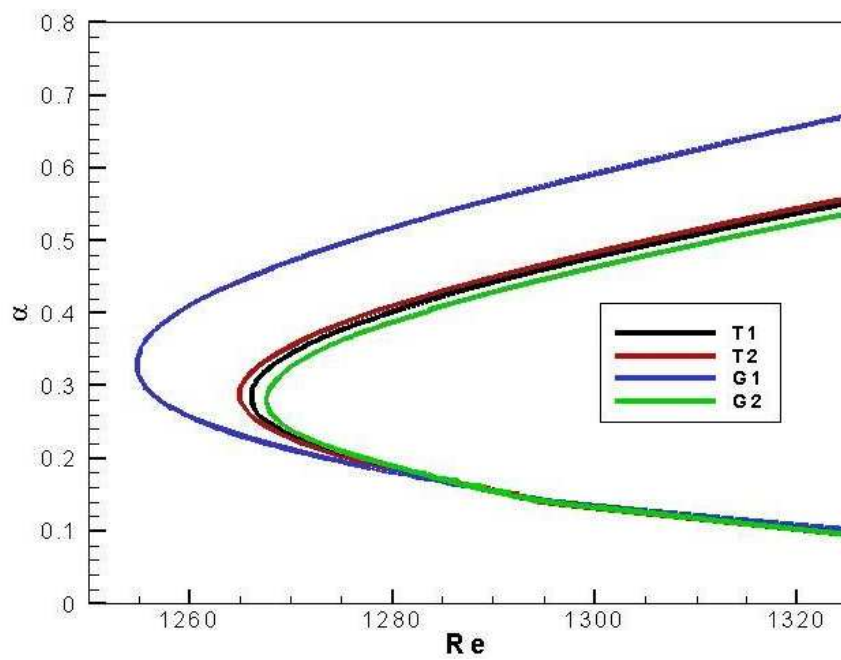


Figure C.5 Neutral stability curves for $d_2^* = 1.8$ mm. at 0°C for sample fluids

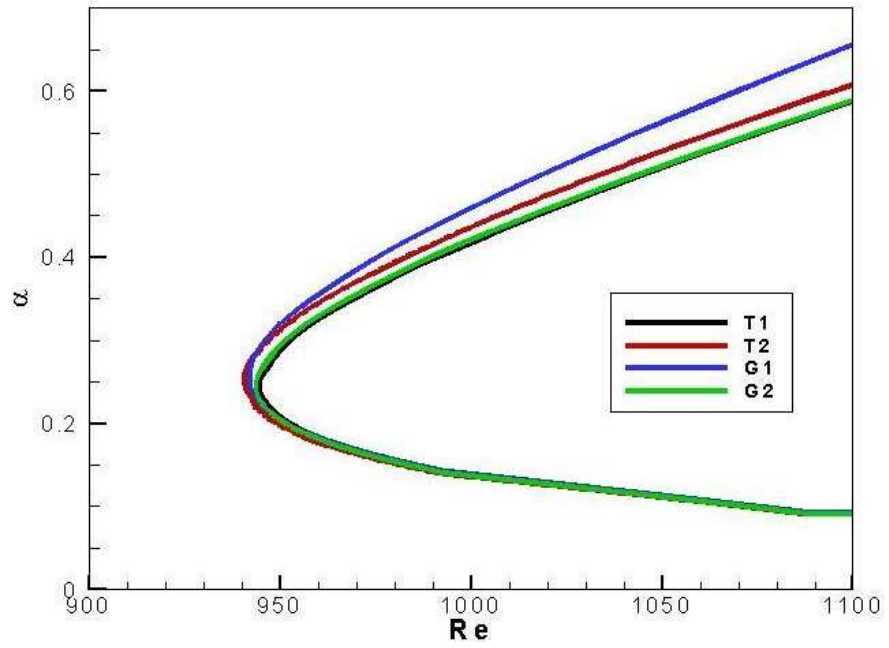


Figure C.6 Neutral stability curves for $d_2^* = 1.2$ mm. at 0°C for sample fluids

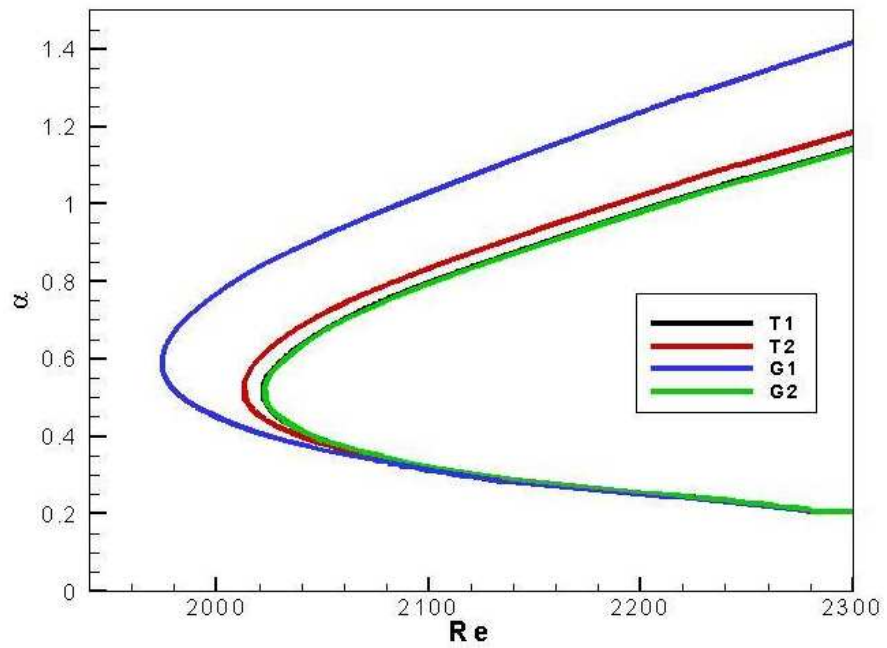


Figure C.7 Neutral stability curves for $d_2^* = 2.4$ mm. at -10°C for sample fluids

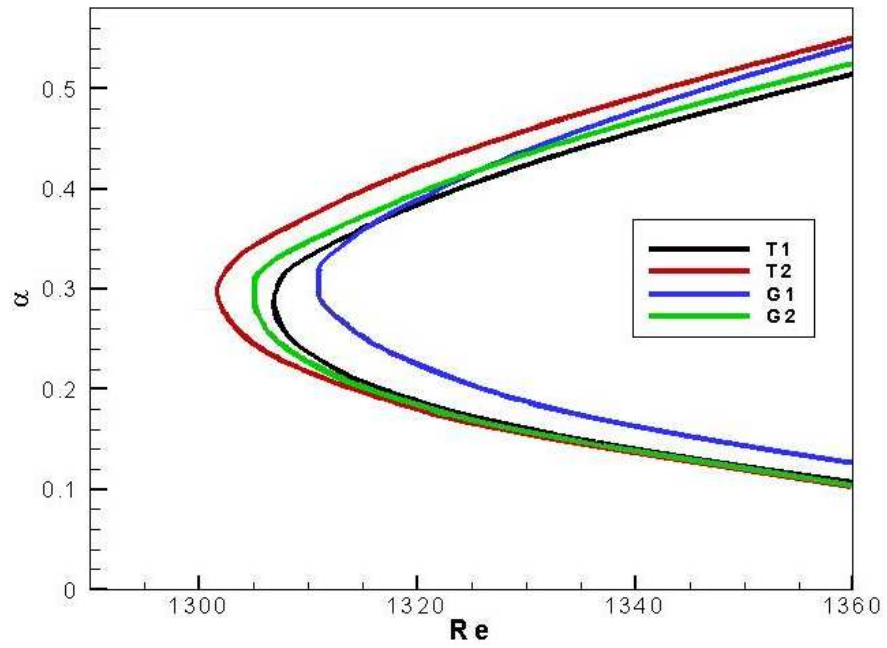


Figure C.8 Neutral stability curves for $d_2^* = 1.8$ mm. at -10 °C for sample fluids

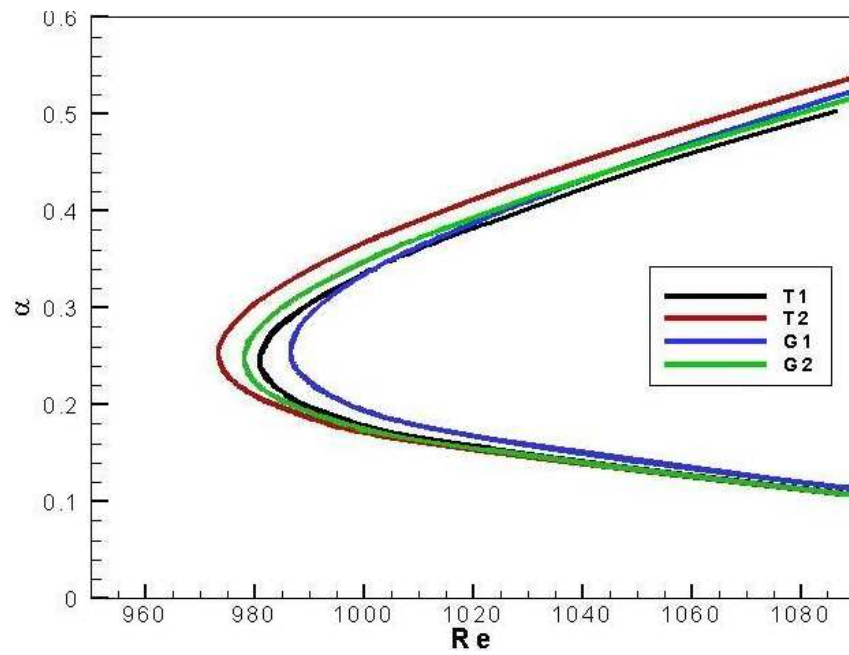


Figure C.9 Neutral stability curves for $d_2^* = 1.2$ mm. at -10 °C for sample fluids